Monthly Notices
of the
ROYAL ASTRONOMICAL SOCIETY

Mon. Not. R. Astron. Soc. **402,** 620–640 (2010) doi:10.1111/j.1365-2966.2009.15915.x

Post-common envelope binaries from SDSS – VII. A catalogue of white dwarf-main sequence binaries

A. Rebassa-Mansergas,[1,2⋆] B. T. Gänsicke,[2] M. R. Schreiber,[1] D. Koester[3] and P. Rodríguez-Gil[4,5,6]

[1]*Departamento de Física y Astronomía, Universidad de Valparaíso, Avenida Gran Bretana 1111, Valparaíso, Chile*
[2]*Department of Physics, University of Warwick, Coventry CV4 7AL*
[3]*Institut für Theoretische Physik und Astrophysik, University of Kiel, 24098 Kiel, Germany*
[4]*Isaac Newton Group of Telescopes, Apdo. de Correos 321, E-38700 Santa Cruz de La Palma, Spain*
[5]*Instituto de Astrofísica de Canarias, Vía Láctea, s/n, La Laguna, E-38205 Tenerife, Spain*
[6]*Departamento de Astrofísica, Universidad de La Laguna, E-38206 La Laguna, Tenerife, Spain*

Accepted 2009 October 21. Received 2009 October 21; in original form 2009 July 30

ABSTRACT

We present a catalogue of 1602 white-dwarf–main-sequence (WDMS) binaries from the spectroscopic Sloan Digital Sky Survey Data Release 6 (SDSS DR6). Among these, we identify 440 as new WDMS binaries. We select WDMS binary candidates by template fitting all 1.27 million DR6 spectra, using combined constraints in both χ^2 and signal-to-noise ratio. In addition, we use *Galaxy Evolution Explorer* (*GALEX*) and UKIRT Infrared Sky Survey (UKIDSS) magnitudes to search for objects in which one of the two components dominates the SDSS spectrum. We use a decomposition/fitting technique to measure the effective temperatures, surface gravities, masses and distances to the white dwarfs, as well as the spectral types and distances to the companions in our catalogue. Distributions and density maps obtained from these stellar parameters are then used to study both the general properties and the selection effects of WDMS binaries in the SDSS. A comparison between the distances measured to the white dwarfs and the main-sequence companions shows $d_{\rm sec} > d_{\rm wd}$ for approximately one-fifth of the systems, a tendency already found in our previous work. The hypothesis that magnetic activity raises the temperature of the inter-spot regions in active stars that are heavily covered by cool spots, leading to a bluer optical colour compared to inactive stars, remains the best explanation for this behaviour. We also make use of SDSS–*GALEX*–UKIDSS magnitudes to investigate the distribution of WDMS binaries, as well as their white-dwarf effective temperatures and companion star spectral types, in ultraviolet to infrared colour space. We show that WDMS binaries can be very efficiently separated from single main-sequence stars and white dwarfs when using a combined ultraviolet, optical and infrared colour selection. Finally, we also provide radial velocities for 1068 systems measured from the Na I λλ8183.27, 8194.81 absorption doublet and/or the Hα emission line. Among the systems with multiple SDSS spectroscopy, we find five new systems exhibiting significant radial velocity variations, identifying them as post-common-envelope binary candidates.

Key words: stars: AGB and post-AGB – binaries: close – binaries: spectroscopic – stars: low-mass, brown dwarfs – white dwarfs.

1 INTRODUCTION

Binaries containing a white-dwarf primary plus a main-sequence companion were initially main-sequence binaries in which the more massive star evolved through the giant phase and became a white dwarf. In the majority of cases, the initial separation of the main-sequence binary is wide enough to allow the evolution of both stars as if they were single.

A small fraction is believed to undergo a phase of dynamically unstable mass transfer once the more massive star is on the giant branch or the asymptotic giant branch (Webbink 1984; de Kool 1992; Willems & Kolb 2004). As a consequence of this mass transfer, the envelope of the giant will engulf its core and the companion

⋆E-mail: arebassa@dfa.uv.cl

star, i.e. the system is entering a common-envelope (CE) phase (e.g. Livio & Soker 1988; Iben & Livio 1993; Taam & Sandquist 2000; Webbink 2008). Friction inside this envelope causes a rapid decrease of the binary separation. Henceforth orbital energy and angular momentum are extracted from the binary orbit and lead to the ejection of the envelope, exposing a post-common-envelope binary (PCEB). As a consequence the orbital period distribution of white-dwarf–main-sequence (WDMS) binaries is clearly bi-modal, with PCEBs concentrated at short orbital periods, and wide WDMS binaries (non-PCEBs) at long orbital periods (Willems & Kolb 2004). After the ejection of the envelope, close WDMS binaries evolve to shorter orbital periods through angular momentum loss via magnetic braking and/or through the emission of gravitational waves. WDMS binaries include progenitors of a wide range of astronomical objects such as cataclysmic variables and super-soft X-ray sources, with some of these objects likely evolving at later stages into Type Ia supernova.

Population synthesis models have been developed for a variety of binary stars undergoing CE evolution (Dewi & Tauris 2000; Nelemans & Tout 2005; Politano & Weiler 2006, 2007; Davis et al. 2008; Davis, Kolb & Willems 2009). However, the theoretical understanding of both CE evolution and magnetic braking is currently poorly constrained by observations (Schreiber & Gänsicke 2003), and progress on this front is most likely to arise from the analysis of a large sample of PCEBs that are well understood in terms of their stellar components. WDMS binaries appear most promising in that respect, as their stellar components are relatively simple, and the Sloan Digital Sky Survey (SDSS; York et al. 2000; Stoughton et al. 2002; Abazajian et al. 2009) offers the possibility of dramatically increasing the number of WDMS binaries available for detailed follow-up studies. Up to date there exist four compilations of SDSS WDMS binaries, namely Eisenstein et al. (2006) (obtained as part of their search of white dwarfs), Silvestri et al. (2007) [which also contains Raymond et al. 2003; Silvestri et al. 2006 as a subset, and was claimed to be complete for SDSS Data Release 5 (DR5)], Augusteijn et al. (2008) (obtained from SDSS DR5 using colour cuts plus proper motions) and Heller et al. (2009) (obtained from a search for sdB stars in SDSS DR6).

Here we initiate a comprehensive study to compile a master sample of spectroscopic WDMS binaries from the SDSS. In this first publication, we make use of the SDSS spectroscopic DR6 (Adelman-McCarthy et al. 2008) to create a catalogue of 1602 WDMS binaries and candidates that were serendipitously observed. This list is not only a superset of all those previous SDSS WDMS binary compilations, but also includes 440 new WDMS binaries. In addition we provide a coherent analysis of the system parameters of both stellar components as well as an extension to *Galaxy Evolution Explorer* (*GALEX*)/UKIRT Infrared Sky Survey (UKIDSS) colours to study the properties of SDSS WDMS binaries. In a parallel effort, and as part of the SDSS Extension for Galactic Understanding and Exploration (SEGUE), some of us carried out a dedicated programme to identify ∼300 WDMS binaries containing cold white dwarfs (Schreiber, Nebot Gomez-Moran & Schwope 2007), a population clearly under-represented in previous samples of WDMS binaries. A detailed analysis of the SEGUE population of WDMS binaries is underway (Schreiber et al., in preparation). Finally, we plan to summarize our efforts by presenting the WDMS binary content of the final SDSS DR7 (Abazajian et al. 2009). This last paper will be accompanied by a public online data base of WDMS binaries.

The final master sample of 'all' spectroscopic SDSS WDMS binaries will form a superb data base for future follow-up studies of WDMS binaries. In particular, analysing the fraction and the characteristics of the PCEBs among the WDMS binaries may provide strong constraints on current theories of compact binary evolution (Rebassa-Mansergas et al. 2007, 2008; Schreiber et al. 2008; Nebot Gómez-Morán et al. 2009; Pyrzas et al. 2009; Schwope et al. 2009).

The structure of the paper is as follows. In Section 2 we present our method of identifying WDMS binaries, and estimate the completeness of the sample in Section 3. In Section 4, we provide our final catalogue. Using a spectral decomposition/model atmosphere analysis, we derive white-dwarf effective temperatures, surface gravities, masses, companion star spectral types and distances in Section 5. We compare these stellar parameters to those obtained in other studies in Section 7, and study the selection effects of WDMS binaries within the SDSS in Section 8. We then provide colour–colour diagrams and colour–colour cuts for WDMS binaries in Sections 9 and 10, respectively. We finally measure the Na I λλ8183.27, 8194.81 absorption doublet and/or the Hα emission radial velocities in Section 11, and summarize our results in Section 12.

2 IDENTIFICATION OF WDMS BINARIES IN THE SDSS

2.1 Computational method

We have developed a procedure based on χ^2 template fitting in order to automatically identify WDMS binary candidates from the SDSS DR6 spectroscopic data base (Adelman-McCarthy et al. 2008). Our initial template set consisted of several dozen SDSS spectra of confirmed WDMS binaries from Eisenstein et al. (2006) and Silvestri et al. (2007). These spectra were chosen to sample a broad range in white-dwarf temperatures and subtypes (DA, DB and DC) as well as companion star spectral types, and to be of a high signal-to-noise ratio (S/N). A set of representative templates is shown in Fig. 1. In addition, we compiled a set of 17 single DA white-dwarf template spectra from Eisenstein et al.'s (2006) list, covering the entire observed range of $T_{\rm eff}$ and $\log g$ as well as the M0–M9 Bochanski et al. (2007) M-dwarf templates.

Each of these WDMS binary, white-dwarf and M-dwarf templates were then fitted to the full 1.27 million spectra in DR6. In this process, the template spectrum was normalized to the SDSS spectrum under scrutiny, and a reduced χ^2 was calculated using the flux errors of the two spectra added in quadrature. In practice, our fitting procedure produced for each of the WDMS binary, white-dwarf and M-dwarf templates a list of spectrum identifier (MJD–PLT–FIB), S/N of the spectrum and χ^2 for all SDSS DR6 spectra. For each of the templates, we plotted χ^2 as a function of the S/N of the target spectrum (see Fig 2) and defined a power-law relation $\chi^2_{\rm max} = a \times {\rm S/N}^b$. We considered any spectrum with

$$\chi^2_{\rm spec} < \chi^2_{\rm max} \quad (1)$$

as a candidate WDMS binary, white dwarf or M-dwarf (depending on the current template). The S/N-dependent form of $\chi^2_{\rm max}$ accounts for the increase of χ^2 for higher values of the S/N. This constraint had to be defined individually for each of the templates, as the different spectral shapes resulted in a large spread of χ^2 distributions. The (χ^2, S/N) planes obtained from fitting the SDSS spectra are shown for two different WDMS binary templates in Fig. 2.

After a first run through the DR6 spectra, we complemented the template set with the spectra of a number of newly identified WDMS binaries and re-ran the fitting for those new templates again. This process was repeated until no new WDMS binary candidates were

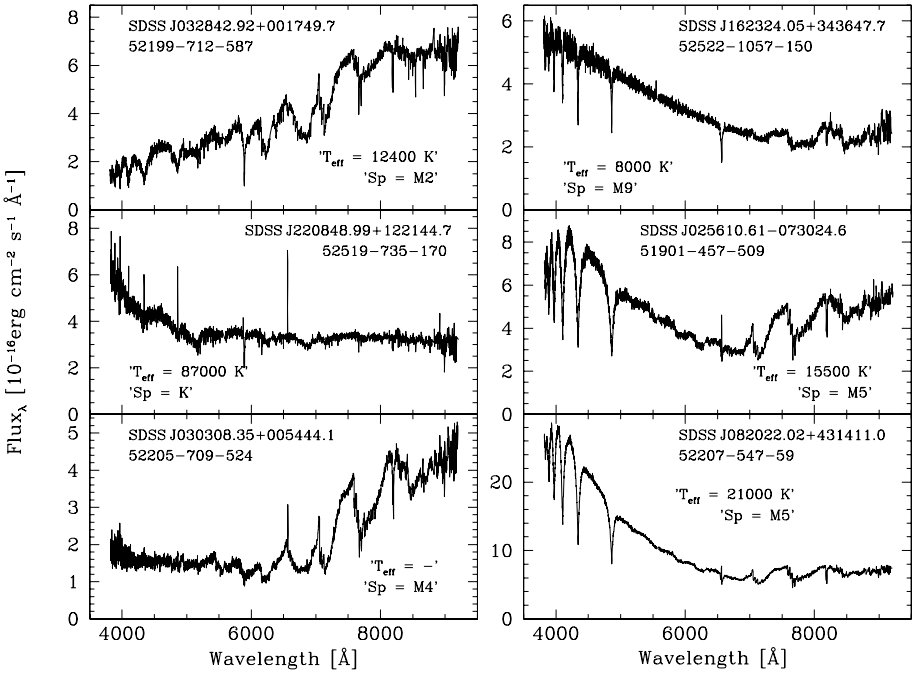

Figure 1. Six examples of previously known WDMS binaries used in this work as WDMS binary templates. SDSS names and MJD–PLT–FIB identifiers are indicated for each of them. White-dwarf effective temperatures and spectral type of the companions (see Section 5) are also indicated in each panel.

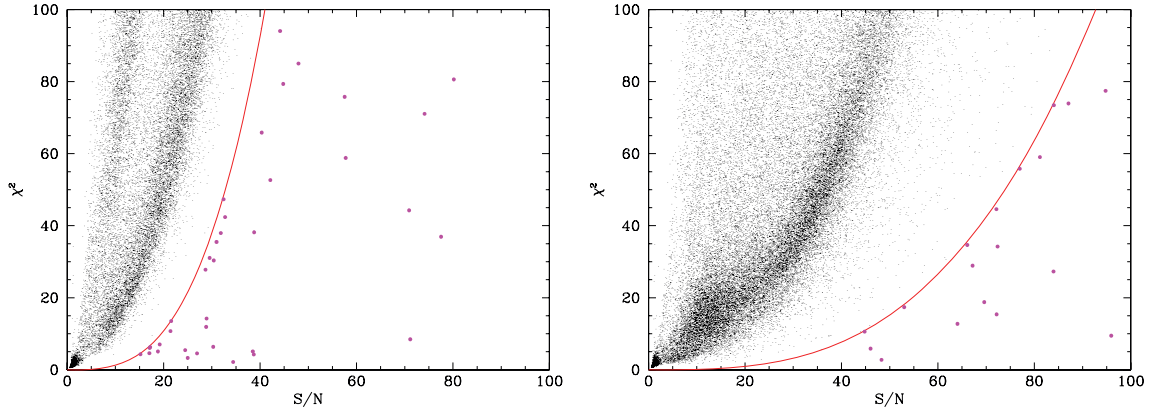

Figure 2. χ^2–S/N plane obtained by fitting two of our WDMS binary templates (left: SDSS J103121.97+202315.1, right: SDSS J204431.44−061440.2) to the entire SDSS spectra data base. Objects falling in the area defined by $\chi^2_{\rm spec} < a \times {\rm S/N}^b$ were considered WDMS binary candidates. Left-hand panel: $\chi^2_{\rm spec} < 0.001 \times {\rm S/N}^{3.1}$. Right-hand panel: $\chi^2_{\rm spec} < 0.0001 \times {\rm S/N}^{3.05}$. WDMS binary candidates are shown in magenta and the equation $\chi^2_{\rm spec} < a \times {\rm S/N}^b$ defined for each template is shown in red.

found – at which point we had used a total of 163 different WDMS binary template spectra.

Even though the above method efficiently identifies WDMS binary candidates among the spectra in DR6, the choice of $\chi^2_{\rm max}$ alone does not completely avoid the filtering of other astronomical objects, such as quasars, main-sequence stars and galaxies. In addition, for templates that are dominated by the white dwarf (M-dwarf), the list of candidates will unavoidably contain a substantial number of single white dwarfs (M-dwarfs). Hence, we first visually inspected all WDMS binary candidates, as well as the white-dwarf and M-type star subsamples (a total of ∼70 000 spectra), and removed those objects that were not of our interest, i.e. neither WDMS binary, white-dwarf or M-dwarf candidates. The final result of the template fitting was a list of 1491 WDMS binary candidates, 8368 single white-dwarf candidates and 15 379 single M-dwarf candidates. It is worth mentioning that we found here 36 WDMS binaries that were observed only/first by SEGUE, and consequently decided to include them in the SEGUE list of WDMS binaries (Schreiber et al. in preparation).

2.2 Red and blue excess in SDSS spectra: help from *GALEX* and UKIDSS

While the template fitting proved to be a robust method to find WDMS binaries in which both stellar components contribute clearly visible amounts of flux, the procedure is prone to misclassify white-dwarf-dominated WDMS binaries as single white dwarfs and M-dwarf-dominated WDMS binaries as single M-dwarfs. We therefore decided to probe more specifically for the presence of excess flux at the red (blue) end of the SDSS spectra in objects classified initially as single white dwarfs (M-dwarfs).

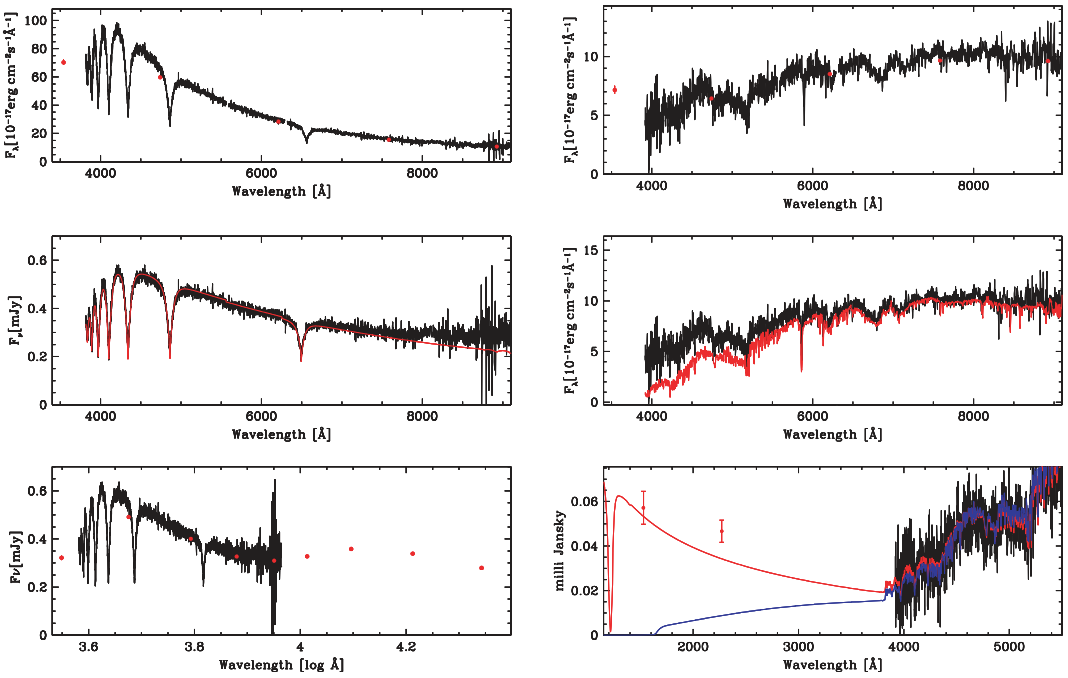

Figure 3. Top left: SDSS spectrum of SDSS J132925.21+123025.5, a WDMS binary candidate initially catalogued as a single DA white dwarf. The red dots represent the SDSS magnitudes. Middle left-hand panel: the best white-dwarf model fit is superimposed in red, unambiguously identifying the red excess of the binary. Bottom left-hand panel: SDSS and UKIDSS magnitudes superimposed to the SDSS spectrum. Again, the UKIDSS magnitudes clearly show the presence of a low-mass companion. Top right-hand panel: the same for SDSS J131928.80+580634.2, an initially catalogued early M-type star. Middle and bottom right-hand panels: the best M-type fit and the ultraviolet *GALEX* magnitudes clearly confirm the presence of a white-dwarf primary, respectively. The red and blue straight lines represent the white-dwarf solutions (red for the hot and blue for the cold) obtained from decomposing/fitting the spectrum (see Section 5).

For the search of red flux excess in single white-dwarf candidates, we fitted synthetic white-dwarf spectra computed with the code described by Koester et al. (2005) to the SDSS spectra and then calculated the reduced χ^2 over the wavelength ranges of 4000–7000 Å ($\chi^2_{\rm b}$) and 7000–9000 Å ($\chi^2_{\rm r}$). Objects with $\chi^2_{\rm r}/\chi^2_{\rm b} > 1.5$ were 'promoted' from single white-dwarf candidates to WDMS binary candidates.

The search for blue flux excess proceeded in an analogous fashion for the single M-dwarf candidates, only that we used the set of high S/N M-dwarf templates from Rebassa-Mansergas et al. (2007) instead of model spectra and calculated the reduced χ^2 over the wavelength ranges of 4000–5000 and 7000–9000 Å. Objects with $\chi^2_{\rm b}/\chi^2_{\rm r} > 1.5$ were 'promoted' from single M-dwarf candidates to WDMS binary candidates.

On the top left-hand and right-hand panels of Fig. 3, we show the SDSS spectra (black line) and SDSS magnitudes (red dots) of SDSS J132925.21+123025.5 and SDSS J131928.80+580634.2, along with the best-fitting white-dwarf model and M-dwarf template (red lines, middle panels). These two objects were initially classified by our template fitting procedure as single white-dwarf and single M star candidates, respectively, but 'promoted' to WDMS binary candidates by the flux excess measurement as described above. The flux excess is more obvious when plotting F_ν (middle left-hand panel) instead of F_λ (top left-hand panel). However, in several cases, the detection of blue or red flux excess is rather marginal.

As a final step in our search for WDMS binaries, we have cross-correlated our entire list of WDMS binary candidates with *GALEX* (Martin et al. 2005; Morrissey et al. 2005) DR 4, providing near- and far-ultraviolet (nuv, fuv) magnitudes, and with the DR 4 of UKIDSS (Dye et al. 2006; Hewett et al. 2006; Lawrence et al. 2007), providing infrared *yJHK* magnitudes. We then inspected the observed ultraviolet–optical spectral energy distribution of all secondary-star-dominated WDMS binary candidates and the optical–infrared spectral energy distribution of all white-dwarf-dominated WDMS binary candidates. Objects where a clear ultraviolet or infrared excess was detected were then included in our WDMS binary sample.

For SDSS J132925.21+123025.5, the UKIDSS magnitudes unambiguously confirm the existence of a low-mass companion (bottom left-hand panel of Fig. 3). Similarly, the ultraviolet *GALEX* magnitudes clearly confirm the presence of a white-dwarf primary in SDSS J131928.80+580634.2 (bottom right-hand panel of Fig. 3).

2.3 SDSS images

As a final check on the nature of the WDMS binary candidates, we inspected their SDSS DR6 images for morphological problems and found primarily two types of issues.

First, single white dwarfs (M-dwarfs) may occasionally be located close to very bright M-dwarfs (white dwarfs or A stars) causing scattered light to enter the spectroscopic fibre resulting in an (apparent) two-component spectrum. A spectacular example is SDSS J073531.86+315015.2 (left-hand panels of Fig. 4): the SDSS spectrum clearly exhibits an M-dwarf at red wavelengths and a blue component with strong Balmer lines in the blue; however, the SDSS image reveals that this is a single M-dwarf at a distance of 12 arcmin of Castor A/B – two $V = 1.88$ and $V = 2.96$ A stars. The SDSS magnitudes (red dots) are superimposed to the SDSS spectrum (black) and are consistent with a single red star. Single M-dwarfs are also likely to be found superimposed with single early-type stars in the

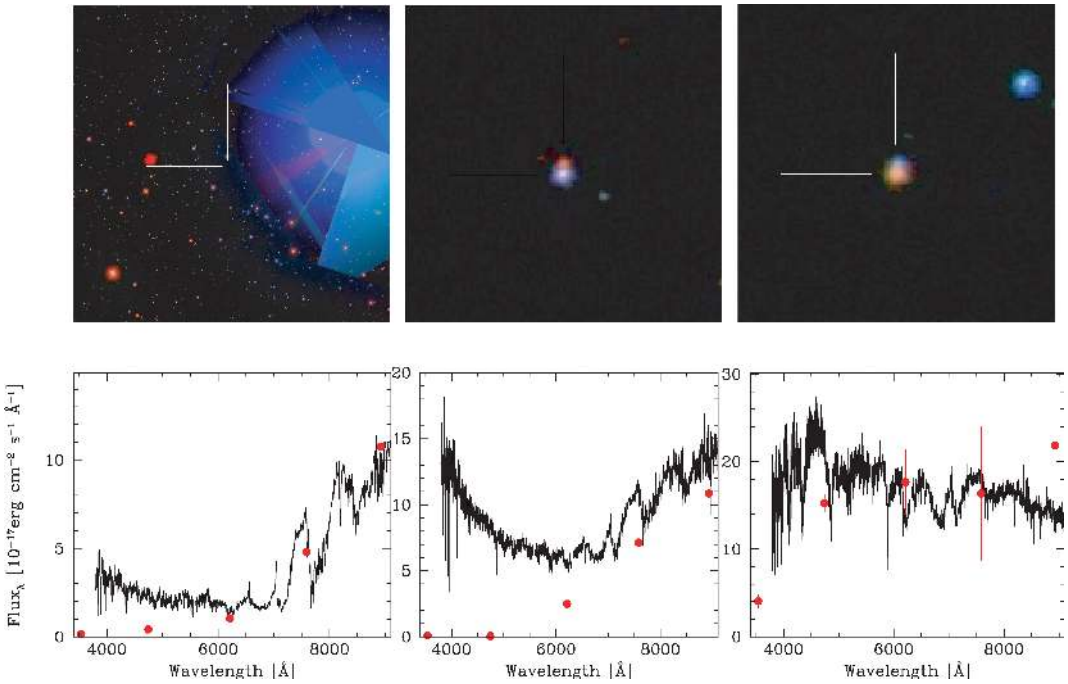

Figure 4. SDSS images of three WDMS binary candidates. Top left-hand panel: SDSS image of SDSS J073531.86+315015.2 (30×30 arcmin^2), a single red star initially considered as a WDMS binary candidate. Bottom left-hand panel: SDSS magnitudes (red dots) and spectrum (black line) of the same system. The light from the saturated bright star (Castor A/B) is also dispersed in the spectrum. The magnitudes are consistent with a single red star. Top middle panel: SDSS image of SDSS J005827.24+005642.6 (1×1 arcmin^2). The image suggests a resolved WDMS binary pair. Middle bottom panel: the detection of the Balmer lines typical of an early F star in the blue, together with the typical spectral features of a low-mass main-sequence star in the red (black solid line), indicates that these are two single stars superimposed in the same image rather than a resolved WDMS binary pair. SDSS magnitudes are indicated with red dots, and are consistent with those of a low-mass star. Top right-hand panel: SDSS image of SDSS J025306.37+001329.2 (1×1 arcmin^2), a resolved WDMS binary in our sample. Bottom right-hand panel: SDSS magnitudes (red dots) and spectrum (black line) of the same system. Whilst the SDSS spectrum clearly shows both components, the SDSS magnitude errors are untypically large due to unsuccessful deblending of the close pair.

same figure. An example is SDSS J005827.24+005642.6 (see the middle top panel of Fig. 4). At first glance, one could be tempted to consider it a spatially resolved WDMS binary pair. However, the SDSS spectrum (middle bottom panel of the same figure) shows the typical Balmer lines of an early F star in the blue, while at redder wavelengths the typical spectral features of a low-mass star can be seen. The large difference in absolute magnitudes between the two spectral types implies that these two stars are a chance superposition along the line of sight, and not a physical binary.

Secondly, SDSS images can help in identifying WDMS binaries among our sample that are spatially resolved, but close enough that flux from both stars will enter into the spectroscopic fibre. In such cases, the SDSS magnitudes are often discrepant with the flux-calibrated SDSS spectrum and/or have large errors as a consequence from the deblending applied by the photometric pipeline. Fig. 4 (top right-hand panel) shows the SDSS image of SDSS J025306.37+001329.2, which reveals a spatially resolved pair of red and blue stars. The SDSS spectrum of SDSS J025306.37+001329.2 contains the typical signatures of a WDMS binary, i.e. broad Balmer lines from the white-dwarf and TiO absorption bands from the M-dwarf; however, the errors on the SDSS magnitudes are untypically large and do not match well the flux-calibrated SDSS spectrum.

2.4 Cross-checks with previous WDMS binary catalogues

A total number of 1491 WDMS binary candidates were identified in Section 2.1. From the analysis carried out in Sections 2.2 and 2.3, we have identified 94 and 89 WDMS binaries by their blue and red excess, respectively, while 115 WDMS binary candidates were removed after inspecting their SDSS images. This increased the number of systems to 1559 WDMS candidates in the spectroscopic SDSS DR6 data base.

Table 1. Comparison of the WDMS binaries identified here with those provided in previous publications. $N_{\rm WDMS}$ gives the number of objects listed, $N_{\rm ident}$ the number of WDMS binaries we have identified within the list, $N_{\rm remov}$ the number of objects we do not consider being WDMS binaries and $N_{\rm lost}$ the number of systems that we have missed (the percentage is given in brackets).

Publication	$N_{\rm WDMS}$	$N_{\rm ident}$	$N_{\rm remov}$	$N_{\rm lost}$
van den Besselaar et al. (2005)	15	15	–	– (0 per cent)
Silvestri et al. (2007)	1225	996	204	25 (2 per cent)
Augusteijn et al. (2008)	130	110	16	4 (3 per cent)
Heller et al. (2009)	636	554	81	1 (0.1 per cent)

In order to evaluate the efficiency of our procedure we compared our results to five previously published lists of WDMS binaries from the SDSS, namely van den Besselaar et al. (2005), Eisenstein et al. (2006), Silvestri et al. (2007) (which includes the systems from Raymond et al. 2003; Silvestri et al. 2006 as a subset), Augusteijn et al. (2008) and Heller et al. (2009). This comparison is summarized in Table 1.

The 15 WDMS binaries containing DB (13) and DC (2) white dwarfs presented by van den Besselaar et al. (2005) have been successfully identified as WDMS binaries with our template fitting algorithm.

Table 2. Updated classification of the 204 objects from Silvestri et al. (2007) which are not considered as WDMS binaries by us. The complete table can be found in the electronic version of the paper (see Supporting Information).

Object	Classification
SDSS J001324.33−085021.4	M star + ?
SDSS J003839.36+260258.5	G star
SDSS J005714.52−000755.8	M star
SDSS J005827.24+005642.6	MS+MS superposition
SDSS J012516.98−010944.2	M star
–	–

Table 3. Updated classification of the 81 objects from Heller et al. (2009) which are not considered as WDMS binaries by us. The complete table can be found in the electronic version of the paper (see Supporting Information).

Object	Classification
SDSS J013007.13+002635.3	Carbon star
SDSS J020538.10+005835.3	No available spectra, WDMS?
SDSS J023906.69+002916.6	DA
SDSS J025622.18+330944.8	O star?
SDSS J032428.78−004613.8	Quasar
–	–

The WDMS binary sample presented by Eisenstein et al. (2006) is almost entirely contained in the WDMS binary catalogue provided by Silvestri et al. (2007) (see below for a detailed comparison). Only 10 objects of Eisenstein et al. (2006) with available SDSS spectra are not listed in Silvestri et al. (2007), and our algorithm has successfully identified these 10 systems as WDMS binaries.

Silvestri et al. (2007) claim that their catalogue contains 1253 objects, but in fact only 1228 spectra (corresponding to 1225 objects) are listed in the electronic edition of their paper and 996 systems of those appear in our catalogue. One is a SEGUE object and will be included in Schreiber et al. (in preparation). The vast majority (i.e. 204) of the remaining 229 objects are not classified as WDMS binaries by us, either because of their spectroscopic appearance or because of morphological problems in the SDSS images. Two examples of misclassified WDMS binaries are the $z = 0.21$ quasar SDSS J032428.78−004613.8 and the $z = 0.11$ galaxy SDSS J114334.70+455134.2. An updated classification of the 204 objects is given in Table 2, whilst the full table is available in the electronic version of this paper (see Supporting Information). The spectra of the 25 genuine WDMS binaries identified by Silvestri et al. (2007), but overlooked by our template fitting algorithm, are dominated by the emission of one of the stellar components. We added these 25 WDMS binaries to our sample.

Augusteijn et al. (2008) developed a WDMS binary identification algorithm based on the SDSS imaging and the proper motion catalogue provided by Gould & Kollmeier (2004). This way, they identified 651 WDMS binary candidates with SDSS *ugriz* photometry, of which 95 are contained in the SDSS DR5 spectroscopic data base. Cross-correlating their full list of 651 objects against the DR6 spectroscopic data base, we find 176 spectra for 130 objects. All but 20 of these objects were in our list. Again, the majority of those systems (16) that have not been identified by our template fitting procedure are not WDMS binaries. We identify nine quasars, three cataclysmic variables, one F star, one M-dwarf one DA white dwarf and one DC white dwarf. The four remaining WDMS binaries have been overlooked by our method because they contain rather cold white dwarfs, and the spectra are dominated by the companions. We added the four systems to our sample.

Recently, Heller et al. (2009) discussed the properties of 636 colour-selected WDMS binaries from SDSS DR6. Most of their systems had been identified previously. Comparing their sample with our catalogue, we find 82 objects missing in our list. Inspecting the SDSS images and spectra (if available) of these 82 systems, we find 81 of them not being WDMS binaries. Two examples are the low-redshift galaxy SDSS J122953.46+473150.3 (U7639; Makarova et al. 1998) and the $z = 0.21$ quasar SDSS J032428.78−004613.8, also included in Silvestri et al. (2007). An updated classification for these 81 objects is provided in Table 3, whilst the complete table is provided in the electronic version of this paper (see Supporting Information). Only one system analysed by Heller et al. (2009) but not in our sample turned out to be a WDMS binary, and we added it to our catalogue.

In summary, comparing the sample of WDMS binaries obtained with our template fitting procedure with previously published catalogues of WDMS binaries shows that our method represents a robust and efficient tool to identify WDMS binaries (Table 1).

3 COMPLETENESS OF THE SAMPLE

In the previous section, we showed that our selection method successfully recovered the vast majority of previously identified SDSS WDMS binaries. In this section, we investigate both the internal completeness of our catalogue, i.e. the fraction of WDMS binaries contained in the DR6 spectroscopic data base that has been identified by our algorithm, and the external completeness, i.e. the fraction of point sources for which SDSS *ugriz* photometry is available that has been spectroscopically observed by the SDSS. A detailed study of the external (spectroscopic) completeness of WDMS binaries within the SDSS is currently underway, and we use this paper to provide preliminary results on this issue. To that end, we first define three regions in SDSS colour–colour planes: the WDMS binary exclusion region that has been defined by Richards et al. (2002) as part of the quasar fibre allocation algorithm and two small rectangular boxes in the $(g - r, r - i)$ plane that sample a significant population of WDMS binaries in colour space. Particularly, these two boxes were defined to test how the external completeness varies between inside and outside the WDMS exclusion box. The $(u - g, g - r)$, $(g - r, r - i)$ and $(r - i, i - z)$ colour–colour diagrams shown in Fig. 5 illustrate the locations of these regions (WDMS, box 1, box 2). The WDMS binaries in our sample excluding those systems that are classified as candidates only (see Section 4) are shown in black, stellar sources in grey and quasars in light grey. Highlighted in light blue are the white dwarf (WD), A star (A) and WDMS binary exclusion regions defined by Richards et al. (2002). Both the A star and the WDMS binary region in the colour planes are combined with a logical 'and'. Boxes 1 and 2 are defined by $(-0.5 < g - r < -0.2, 0 < r - i < 0.2)$ and $(-0.3 < g - r < 0.1, 0.3 < r - i < 0.5)$, respectively.

To determine the completenesses, we visually classified all SDSS DR6 spectra of point sources with $g \leq 20$ and used the CASJOBS interface (Li & Thakar 2008)[1] to the SDSS data base to determine the number of photometric point sources with clean photometry in each of the regions defined above. The fraction of WDMS binaries identified by the template matching routine among the total number of spectroscopically identified WDMS binaries inside the selected

[1] http://casjobs.sdss.org/CasJobs/

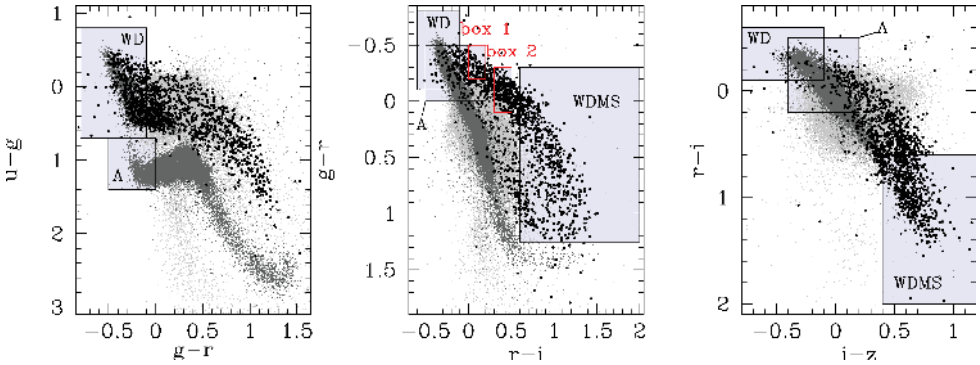

Figure 5. From left to right: the $(u-g, g-r)$, $(g-r, r-i)$ and $(r-i, i-z)$ colour diagrams for the WDMS binaries in our sample (black; excluding WDMS binary candidates), stellar sources (dark grey) and quasars (light grey), respectively. The white-dwarf, A star and WDMS binary exclusion boxes defined by Richards et al. (2002) are shaded in light blue. The regions within the two red boxes in the $(g-r, r-i)$ plane and the WDMS binary exclusion region of Richards et al. (2002) in the $(g-r, r-i)$ and $(r-i, i-z)$ planes are used to estimate the completeness of our WDMS binary sample (see Section 3).

Table 4. We give here the number of SDSS point sources $N_{\rm p}$, the number of available SDSS spectra $N_{\rm spec}$, the number of spectroscopic WDMS binaries $N_{\rm WDMS}$ and the number of WDMS binaries we have identified $N_{\rm ident}$ for each of the WDMS, box 1 and box 2 regions defined in Section 3. The external completeness is estimated as $N_{\rm spec}/N_{\rm p}$ and the internal completeness as $N_{\rm ident}/N_{\rm WDMS}$.

	Reg.	$N_{\rm p}$	$N_{\rm spec}$	$N_{\rm WDMS}$	$N_{\rm ident}$	Ext. C.	Int. C.
$g \leq 20$	WDMS	8002	575	389	377	7 per cent	97 per cent
	Box 1	708	247	67	67	35 per cent	100 per cent
	Box 2	6689	2280	135	131	34 per cent	97 per cent
$i \leq 19.1$	Box 1	313	188			60 per cent	
	Box 2	2822	1672			60 per cent	
$i \leq 20.1$	Box 1	389	59			15 per cent	
$i > 19.1$	Box 2	13 110	1770			14 per cent	

region gives an estimate of the internal completeness. The external completeness is simply given by the fraction of spectroscopically observed point sources inside a given colour–colour region. In order to evaluate the impact of the brightness limit applied in the quasar selection algorithm (Richards et al. 2002), i.e. a de-reddened $i < 19.1$, we additionally performed the external completeness analysis for the ranges $i \leq 19.1$ and $19.1 < i \leq 20.1$ outside the WDMS exclusion box, i.e. for boxes 1 and 2. The results are given in Table 4 and can be summarized as follows.

(i) SDSS DR6 contains 8002 photometric point sources with $g \leq 20$ inside the Richards et al. (2002) WDMS binary exclusion box. SDSS spectra are available for 575 (or 7 per cent of the point sources) systems, and we visually classify 389 of these as WDMS binaries. The remaining 186 objects are mostly single M stars but we also identify four cataclysmic variables and eight quasars. The small external spectroscopic completeness of SDSS DR6 (7 per cent) in the WDMS binary box as well as the large number of WDMS binaries (67 per cent) among the spectroscopically observed objects is not surprising, as this region has been explicitly excluded in the quasar selection algorithm (Richards et al. 2002). All but 12 of the 389 WDMS binaries have been successfully identified by our automated template-matching algorithm, which gives an internal completeness of 97 per cent. Among the 12 missing objects, nine contain cool (probably DC) white dwarfs, one contains a clear DA white dwarf, one a clear DC white-dwarf primary and one we identify as a low-accretion-rate polar (LARP; SDSS J204827.90+005008.9; Schmidt et al. 2005). In all the 12 cases, the spectra are dominated by the emission of the companion stars.

(ii) Box 1 contains 708 point sources with $g < 20$ in DR6 and for 247 of these at least one SDSS spectrum is available, corresponding to an external completeness of 35 per cent. As expected, we find the external completeness to significantly change at the i-magnitude limit incorporated in the quasar search algorithm. While it increases to ∼60 per cent for $i \leq 19.1$, it drops to ∼15 per cent for $19.1 < i \leq 20.1$.

Among the 247 objects, 67 (27 per cent) are WDMS binaries. The remaining systems are mainly quasars, a few single white dwarfs, early-type main-sequence stars and two cataclysmic variables. All the 67 WDMS binaries in this box have been identified by our search algorithm (Section 2) equivalent to an internal completeness of 100 per cent.

(iii) SDSS DR 6 contains 6689 SDSS point sources in box 2 and for 2280 of them SDSS spectroscopy is available, which gives an external completeness of 34 per cent using $g < 20$. As for box 1, the quasar limit on the reddening-corrected i-magnitude of 19.1 is very much affecting the external completeness. It increases significantly to ∼60 per cent for $i \leq 19.1$ but decreases to ∼14 per cent for objects fainter than the quasar limit, i.e. for $19.1 < i \leq 20.1$. At first glance, one might consider the spectroscopic completeness of ∼60 per cent for $i \leq 19.1$ to be surprisingly low compared to ∼95 per cent obtained for the quasar selection algorithm (Vanden Berk et al. 2005). However, one should keep in mind that 'outside

the exclusion boxes' is not equivalent to inside the (rather complex) quasar selection. In addition, in DR6 the area followed-up spectroscopically was only $\simeq$82 per cent of the imaging area, implying a systematically lower spectroscopic completeness than expected for DR7. As mentioned earlier, a more complete analysis of the completeness of SDSS WDMS binaries is underway and will be presented in a subsequent publication.

From the 2280 spectra that are available in box 2, only 135 (6 per cent) are WDMS binaries. The vast majority of the remaining objects are quasars, but we also identify some few single main-sequence stars and one cataclysmic variable. All but four of the 135 WDMS binaries have been found by our template fitting method, corresponding to an internal completeness of 97 per cent. The four systems that have not been identified by our algorithm are SDSS J110539.77+250628.6, which is in fact the semidetached magnetic cataclysmic variable ST LMi observed during a deep low state; SDSS J124959.76+035726.6, a typical WDMS binary previously listed as a cataclysmic variable candidate by Szkody et al. (2004); SDSS J150954.40+243449.3, which has a broken SDSS spectrum; and SDSS J204218.52−065638.4, a spatially resolved main-sequence-dominated WDMS binary.

Three main conclusions can be drawn from the analysis carried out in Fig. 5. First, the spectroscopic completeness in the SDSS is much larger in quasar-dominated colour–colour space, i.e. 34 per cent in box 2 compared to only 7 per cent in the WDMS binary exclusion box of Richards et al. (2002). The low completeness in the WDMS binary exclusion box, combined with the high fraction of WDMS binaries among all objects in this region (67 per cent), implies that the number of SDSS WDMS binaries could be dramatically increased by additional follow-up spectroscopy of point sources located in this box. Since the spectroscopic completeness in the WDMS binary exclusion box is 7 per cent, and only 389 WDMS binaries benefit from spectra, this then implies that the SDSS did not target $\sim$5500 WDMS binaries for follow-up spectroscopy within this region. As partners of SEGUE, some of us performed such a programme and identified $\sim$300 new WDMS binaries (Schreiber et al. 2007). Secondly, outside the exclusion boxes the external completeness drops significantly from $\sim$60 to $\sim$15 per cent at the *i*-magnitude limit of 19.1 implemented in the quasar search algorithm. Finally, and most importantly, only 16 WDMS binaries (four in box 2 and 12 in the WDMS binary exclusion box) have not been identified by our template fitting routine. Assuming that the three analysed colour boxes are representative for the entire WDMS binary bridge, we derive an internal completeness of $\sim$98 per cent of our catalogue. Virtually all the systems our search algorithm failed to identify are dominated by the emission of the secondary star. Such systems are therefore expected to form the remaining $\sim$2 per cent of WDMS binaries contained in the SDSS DR6 data base.

The 16 WDMS binaries that we previously overlooked have been added to our sample that now forms our final SDSS DR6 WDMS catalogue, as described in the following section.

4 THE FINAL CATALOGUE

From the analysis described in Sections 2 and 3, a total number of 1602 WDMS binaries have been identified. These systems form our final catalogue of SDSS DR6 WDMS binaries and WDMS binary candidates. We describe in this section the main tables characterizing our sample. An excerpt of each table is given here, while the complete tables can be found in the electronic version of the paper (see Supporting Information).

In Table 5, we list the coordinates, *GALEX* DR4, SDSS DR6 and UKIDSS DR4 magnitudes. Occasionally, multiple SDSS and *GALEX* magnitudes are available for one system. In these cases, we give averaged magnitudes. We used point spread function (PSF) SDSS magnitudes when available and fibre magnitudes otherwise. *GALEX* magnitudes are available for 1327 WDMS binaries and UKIDSS magnitudes for 466.

In Table 6, we provide relative numbers of the stellar components in our WDMS binary catalogue. For the white dwarfs, we use flags DA, DB, DC, WD (if the white-dwarf type is unknown), DH (if the white dwarf is magnetic) and PG 1159 (hot hydrogen-deficient pre-white dwarf). We use the acronym LARP to indicate a low-accretion-rate polar. The secondary stars are flagged as M or K according to their spectral type. If the flag is followed by a colon, the classification of the stellar component is uncertain. Finally, we list in brackets the WDMS binary candidates. We basically consider two types of candidates: (1) systems with very low S/N ratio spectroscopy that does not allow a clear classification of the stellar

Table 5. The complete catalogue. Coordinates and *GALEX*–SDSS–UKIDSS magnitudes for the 1602 WDMS binaries and candidates are also included. The entire table (including also the photometric errors) is provided in the electronic version of the paper (see Supporting Information). We use '–' to indicate that no magnitude is available.

SDSS J	RA (°)	Dec. (°)	*nuv*	*fuv*	*u*	*g*	*r*	*i*	*z*	*y*	*J*	*H*	*K*
000152.09+000644.7	0.46704	0.11242	18.45	17.90	19.03	18.61	17.94	17.50	17.25	16.51	16.05	15.40	15.28
000442.00–002011.6	1.17500	−0.33656	–	–	23.72	20.38	19.13	18.65	18.28	–	–	–	–
000611.94+003446.5	1.54975	0.57958	21.78	–	21.38	20.92	20.12	19.00	18.38	17.53	17.05	16.58	16.20
001029.87+003126.2	2.62446	0.52394	20.17	19.96	21.92	20.85	19.97	19.00	18.42	17.65	17.14	16.52	16.36
001247.18+001048.7	3.19658	0.18019	20.50	20.71	20.73	20.21	19.66	18.63	17.96	17.09	16.60	16.13	–
001339.20+001924.3	3.41333	0.32342	16.41	19.73	15.94	15.56	15.55	15.63	15.89	–	–	–	–
001359.39–110838.6	3.49749	−11.14405	17.77	17.42	18.30	18.43	18.31	20.75	22.82	–	–	–	–
001549.02+010937.3	3.95425	1.16036	20.97	20.68	21.23	20.86	20.60	19.85	19.27	18.46	17.86	17.45	17.12
001726.63–002451.1	4.36096	−0.41419	19.71	20.30	19.67	19.28	19.02	18.18	17.54	16.60	16.07	15.56	–
001733.59+004030.4	4.38996	0.67511	20.83	22.43	22.09	20.79	19.58	18.17	17.38	16.37	15.84	15.27	14.97
001749.24–000955.3	4.45517	−0.16536	15.87	15.40	16.56	16.86	17.03	16.78	16.47	15.75	15.33	14.76	14.56
001853.79+005021.5	4.72412	0.83931	20.46	20.27	21.00	20.38	19.64	18.80	18.35	17.52	17.09	16.51	16.27
001855.19+002134.5	4.72996	0.35958	22.42	22.12	21.60	20.60	19.87	18.97	18.38	17.54	17.09	–	–
002143.78–001507.9	5.43242	−0.25219	22.20	–	22.58	19.63	18.39	17.02	16.30	15.40	14.87	14.31	14.05
–	–	–	–	–	–	–	–	–	–	–	–	–	–

Table 6. The catalogue divided into the different WDMS binary subtype, as defined in Section 4.

Type	Number	Type	Number
DA/M	1176	DB/M:	1
DB/M	45	DA:/K	5
DC/M	34	DA/K:	10
DA/K	49	DH/M	1[a]
DB/K	3	LARP	1[b]
WD/M	135	PG1159/M	1[c]
WD/K	26	(WD/M)	32
WD/M:	1	(WD/K)	2
DA:/M	27	(DA/M)	4
DB:/M	1	(DC/M)	1
DC:/M	3	(DA/K)	1
DA/M:	43		

[a]Szkody et al. (2009); [b]Schmidt et al. (2005); [c]Nagel et al. (2006).

components in their spectra and (2) systems with marginal blue (red) excess in their SDSS spectra, without morphological problems in their SDSS images (Section 2.3), and with χ^2 values (Section 2.2) favouring a binary classification but no *GALEX* (UKIDSS) magnitudes available to confirm the existence of the second component.

5 STELLAR PARAMETERS

In Rebassa-Mansergas et al. (2007, 2008) and Schreiber et al. (2008), we presented a spectral decomposition/fitting technique and an M-dwarf spectral-type–radius relation to determine the stellar parameters of WDMS binaries spectroscopically identified by the SDSS. Our method allows us to estimate the effective temperature, surface gravity, mass and radius of the white dwarf as well as the spectral type and radius of the main-sequence companion. In addition, two independent distance estimates can be obtained by estimating the best-fitting flux scaling factors of the two components (see Rebassa-Mansergas et al. 2007 for details). We here basically use the same procedure but incorporate two modifications.

First, we compiled an additional library of 222 high S/N spectra of DB white dwarfs from SDSS DR 4 (Eisenstein et al. 2006) covering the entire range of observed $T_{\rm eff}$. Decomposing the binary spectrum and fitting the stellar components in the same way as in Rebassa-Mansergas et al. (2007) but using the just mentioned DB templates instead of DA templates allows us to estimate the DB effective temperatures in our catalogue.

As a second modification, we take into account the ultraviolet *GALEX* magnitudes if the spectral fitting does not provide a unique solution for the white-dwarf temperatures. An example is given in Figs. 6–8. Performing the spectral decomposition of SDSS J082609.72+194126.3 into the white-dwarf and main-sequence components (Fig. 6) and modelling the Balmer lines of the white-dwarf model fit provide two solutions for the white-dwarf temperature, the so-called cold and hot solutions (black dots in the top right-hand panel of Fig. 7). In most cases, an additional fit to the entire spectrum breaks this ambiguity and clearly indicates which of the two solutions has to be preferred. However, in the case of SDSS J082609.72+194126.3 the ambiguity remains as the fit to the entire spectrum results in values that fall exactly on the line of maximum Hβ-equivalent width. As shown in the bottom panel of Fig. 8, the ultraviolet magnitudes measured by *GALEX* clearly exclude the hot solution.

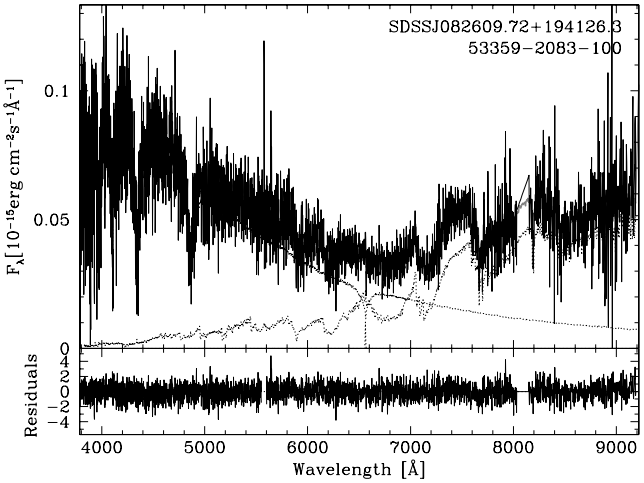

Figure 6. Two-component fits to SDSS J082609.72+194126.3, a WDMS binary in our sample. The top panel shows the WDMS binary spectrum as a black line and the two templates, white dwarf and M-dwarf, as dotted lines. The bottom panel shows the residuals (in units of the standard deviation) from the fit. The SDSS spectrum identifiers MJD, PLT and FIB are given below the object name. See also Figs. 7 and 8.

The stellar parameters and distances obtained for the 1602 WDMS binaries in our catalogue are given in Table 7. Both the cold and the hot solutions are provided for each spectrum, while the solution preferred by us is given in the first line. The complete table is available in the electronic version of the paper (see Supporting Information).

6 DISTRIBUTION OF STELLAR PARAMETERS

We present in this section distributions of surface gravity and effective temperature of the white dwarfs as well as the spectral-type distribution of the companion stars in our catalogue. To facilitate the comparison with previous works, we also provide the distribution of white-dwarf masses. Our template fitting algorithm covers secondary star spectral types M0–M9, and the spectral-type distribution shown here includes only clear classifications in this range. For the distributions of the white-dwarf stellar parameters, we only considered systems with relative errors smaller than 25 per cent. This resulted in 1433, 1198, 1127 and 558 WDMS binaries for the spectral type, surface gravity, effective temperature and white-dwarf mass distributions, respectively (see Fig. 9).

In general terms, the distributions are similar to those presented in Rebassa-Mansergas et al. (2007): the most frequent white-dwarf temperatures range between 10 000 and 20 000 K, white-dwarf masses cluster around $M_{\rm wd} \simeq 0.5\,{\rm M}_{\odot}$, $\log g \simeq 7.8$ for the vast majority of the white dwarfs and the spectral type of the companion stars is typically M3–M4. In Fig. 10, we show the $T_{\rm eff}$, $M_{\rm wd}$, $\log g$ and spectral-type cumulative distributions obtained from the WDMS binaries studied in this work (blue lines), the systems analysed in Rebassa-Mansergas et al. (2007) (red lines) and systems from a volume-limited sample of single white dwarfs (black lines; Holberg et al. 2008). Kolmogorov–Smirnov (KS) tests were applied to compare the sets of effective temperatures, white-dwarf masses and $\log g$. As the secondary spectral-type distribution consists of discrete values, we performed a χ^2 test in this case. We briefly describe each parameter distribution in the following subsections.

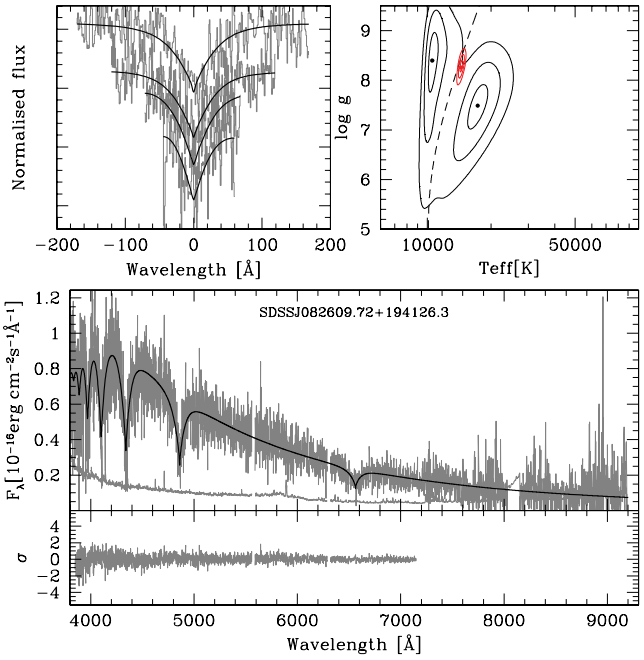

Figure 7. Spectral model fit to the white-dwarf component of SDSS J082609.72+194126.3 obtained after subtracting the best-fitting M-dwarf template. Top left-hand panel: best fit (black lines) to the normalized Hβ to Hϵ (grey lines, top to bottom) line profiles. Top right-hand panels: 3, 5 and 10$\sigma\,\chi^2$ contour plots in the $T_{\rm eff}$–log g plane. The black contours refer to the best line profile fit and the red contours to the fit of the whole spectrum. The dashed line indicates the occurrence of maximum Hβ-equivalent width. The best 'hot' and 'cold' line profile solutions are indicated by black dots and the best fit to the whole spectrum is indicated by a red dot. Bottom panel: the residual white-dwarf spectra resulting from the spectral decomposition and their flux errors (grey lines) along with the best-fitting white-dwarf model (black line) and the residuals of the fit (grey line, bottom). See also Figs 6 and 8.

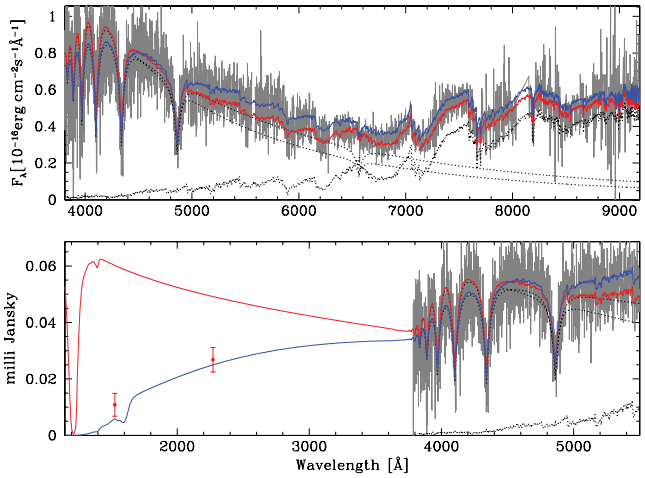

Figure 8. Top: in blue the cold white-dwarf solution obtained in Fig. 7 plus the best-fitting M-dwarf template obtained in Fig. 6; in red the same but for the hot solution; in grey the SDSS spectrum of SDSS J082609.72+194126.3; in black dotted line the best-fitting M-dwarf template, and the white-dwarf models that satisfy the cold and hot solutions in Fig. 7. Bottom: the same but including the near- and far-ultraviolet *GALEX* magnitudes of this object (red dots). See also Figs 6 and 7.

6.1 White-dwarf temperature

We obtain a 40 per cent probability (called KS probability in what follows) for the maximum vertical distance between the white-dwarf temperature distribution obtained here and the distribution in Rebassa-Mansergas et al. (2007) being equal to or larger than the maximum vertical distance between the two cumulative white-dwarf temperature distributions. Hence, there are no indications that the two distributions are not drawn form the same parent population. In contrast, comparing the WDMS binary white-dwarf temperature distribution with the temperature distribution of the volume-limited sample of single white dwarfs (Holberg et al. 2008; black lines in Fig. 10) we obtain a KS probability of 10^{-15}. This is straightforward to understand as the presence of the secondary star makes the identification of cold white-dwarf primaries rather difficult.

6.2 White-dwarf mass and surface gravity

Comparing the white-dwarf mass and surface gravity distributions obtained here with the sample described in Rebassa-Mansergas et al. (2007), we obtain KS probabilities of 50 and 2 per cent, respectively. The low KS probability for the log g distributions is caused by the significantly higher fraction of low-mass white dwarfs in the present sample (see Section 7.1). This is most likely an effect of the systematic changes in the flux calibration pipeline of SDSS spectra. These changes especially affect the blue part in the spectrum and, hence, the fit to the continuum that allows us to distinguish between the hot and cold solutions. In addition, the decision between the hot and cold solutions is affected by taking into account *GALEX* ultraviolet fluxes, one of the modifications incorporated in this paper (see also Section 7.1).

Comparing the distributions obtained with those derived from a volume-limited sample of single white dwarfs (Holberg et al. 2008; black lines in Fig. 10), we obtain KS probabilities of 10^{-12} for the white-dwarf masses and 10^{-15} for the surface gravities. The white-dwarf mass distributions of WDMS binaries and single white dwarfs are indeed expected to be different. The white-dwarf mass distribution of WDMS binaries is composed of two different types of systems, i.e. WDMS binaries with an initial main-sequence binary separation large enough to avoid mass transfer during the evolution of the more massive star and systems that suffer from CE evolution (PCEBs). The white-dwarf mass distribution of the non-interacting WDMS binary population is expected to be identical to the mass distributions of single white dwarfs, i.e. clustering at $M_{\rm wd} \simeq 0.6\,{\rm M}_{\odot}$, while PCEBs are expected to contain a large number of low-mass He-core white dwarfs ($M_{\rm wd} \leq 0.47\,{\rm M}_{\odot}$). For example, de Kool & Ritter (1993) estimate the fraction of such systems among PCEBs to be about 50 per cent. As ∼30 per cent of the presented sample of WDMS binaries from the SDSS have evolved through a CE phase (Schreiber et al. 2008), the rather large fraction of white dwarfs with $M_{\rm wd} \simeq 0.4\,{\rm M}_{\odot}$ in Fig. 9 is not surprising but expected. We are currently pursuing a large-scale follow-up project of WDMS binaries to identify the PCEBs in our sample and to measure their orbital parameters. A detailed analysis of the white-dwarf mass distribution of PCEB and wide WDMS binaries is underway (Rebassa-Mansergas et al., in preparation).

6.3 Secondary star spectral type

The distribution of spectral types is shown in the bottom panel of Fig. 9. The cut-off at early spectral types is very likely a consequence of selection effects as discussed in more detail in Section 8. The strongly decreasing number of WDMS binaries with late-type

Table 7. White-dwarf masses, effective temperatures, surface gravities, spectral types and distances of the 1602 WDMS binaries in our catalogue, as determined from spectral modelling. We list both the hot and the cold solutions, with the preferred solution given in the first line for each spectrum. The other solution is given for completeness. The complete table, including also notes for individual systems, can be found in the electronic version of the paper (see Supporting Information). We use flags *e*, *s*, *a*, and *h* and 're' for those systems which have been studied previously by Eisenstein et al. (2006), Silvestri et al. (2007), Augusteijn et al. (2008) and Heller et al. (2009), and which are resolved WDMS binary pairs, respectively. Again, we indicate that no stellar parameters are measured with '–'.

SDSS J	Type	MJD	PLT	FIB	$T_{\rm eff}$ (K)	err	log g	err	$M_{\rm wd}$ ($M_\odot$)	err	$d_{\rm wd}$ (pc)	err	Sp	$d_{\rm sec}$ (pc)	err	Flag
–	–	–	–	–	–	–	–	–	–	–	–	–	–	–	–	–
013356.07−091535.1	DA/M	53612	1915	431	12 392	1324	7.47	0.36	0.36	0.16	531	112	8	247	100	
013356.07−091535.1	DA/M	53612	1915	431	12 250	1328	7.49	0.36	0.36	0.16	523	110	8	247	100	
013418.52+010100.0	DA/M	53741	1502	517	22 811	2601	7.75	0.41	0.50	0.22	912	224	1	1146	225	re
013418.52+010100.0	DA/M	53741	1502	517	9844	473	8.66	0.46	1.01	0.25	201	73	1	1146	225	
013441.30−092212.7	DA/M	52147	662	477	12 110	2657	7.06	1.13	0.24	0.48	2464	1314	2	1914	456	
013441.30−092212.7	DA/M	52147	662	477	11 699	2808	7.14	1.19	0.26	0.56	2315	1285	2	1914	456	
013441.30−092212.7	WD/M	52178	662	468	–	–	–	–	–	–	–	–	2	1900	453	
013441.30−092212.7	WD/M	52178	662	468	–	–	–	–	–	–	–	–	2	1900	453	
013504.31−085919.0	DA/M	53612	1915	464	9187	480	8.82	0.69	1.10	0.36	218	134	4	471	139	a
013504.31−085919.0	DA/M	53612	1915	464	25 891	4599	7.40	0.77	0.38	0.36	2119	919	4	471	139	a
013716.08+000311.3	DA/M	52203	698	465	18 756	3667	8.52	0.70	0.94	0.37	586	295	2	856	204	s/e
013716.08+000311.3	DA/M	52203	698	465	15 601	5326	8.88	0.95	1.14	0.49	364	326	2	856	204	s/e
013750.03+003237.6	DA/M	52203	698	470	22 292	894	8.38	0.14	0.86	0.08	271	29	2	272	65	s
013750.03+003237.6	DA/M	52203	698	470	16 717	1890	9.24	1.16	1.32	0.60	91	31	2	272	65	s
013801.04+230329.3	DA/M	53341	2064	216	11 835	610	8.13	0.21	0.69	0.14	329	47	7	218	120	s/h
013801.04+230329.3	DA/M	53341	2064	216	15 246	772	7.77	0.18	0.49	0.09	518	56	7	218	120	s/h
013841.09+131257.6	WD/K	51882	426	138	–	–	–	–	–	–	–	–	–	–	–	
013841.09+131257.6	WD/K	51882	426	138	–	–	–	–	–	–	–	–	–	–	–	
–	–	–	–	–	–	–	–	–	–	–	–	–	–	–	–	–

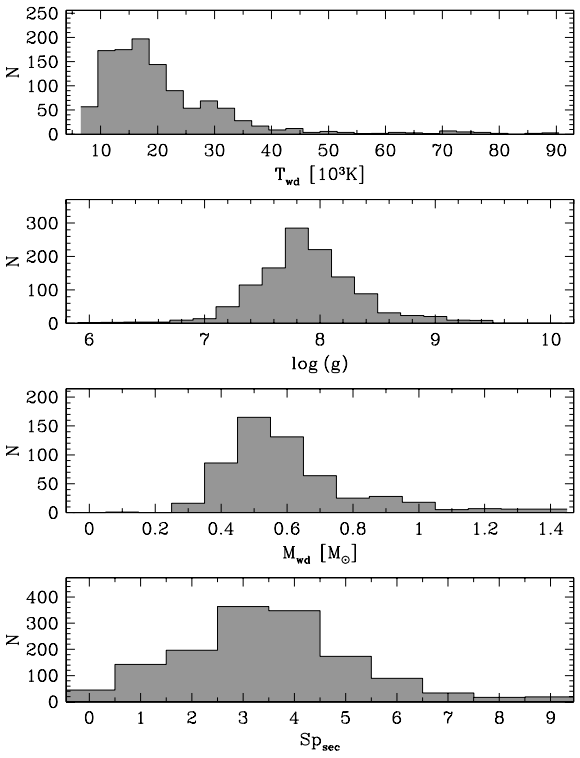

Figure 9. White-dwarf effective temperature, surface gravity and mass, and spectral type of the secondary distributions obtained from the SDSS WDMS binaries in our catalogue.

(M7–M9) companions might also be related to selection effects, as late-type stars are faint and harder to detect against a moderately hot white dwarf. Nevertheless, the SDSS covers a much broader colour space than previous surveys and, in principle, should be able

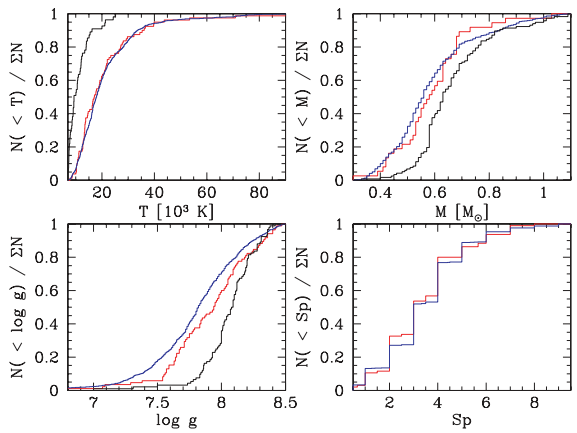

Figure 10. Effective temperature (top left), white-dwarf mass (top right), surface gravity (bottom left) and spectral type (bottom right) cumulative distributions obtained from the stellar parameters of the WDMS binaries presented here (blue lines), analysed in Rebassa-Mansergas et al. (2007) (red lines), and from a volume-limited sample of single white dwarfs (black lines; Holberg et al. 2008).

to identify more WDMS binaries containing cool white dwarfs plus very late-type companions. It is also worth mentioning that Farihi, Becklin & Zuckerman (2005) have constructed the relative distribution of spectral types in the local M/L dwarf distribution, which peaks around M3–M4 and steeply declines towards later spectral types, suggesting that late-type companions to white dwarfs are intrinsically rare (see Section 8 for more details). The χ^2 comparison of the WDMS binary spectral-type distribution presented here with the one described in Rebassa-Mansergas et al. (2007) gives a probability of 82 per cent that both distributions are drawn from the same parent distribution (see also Fig. 10).

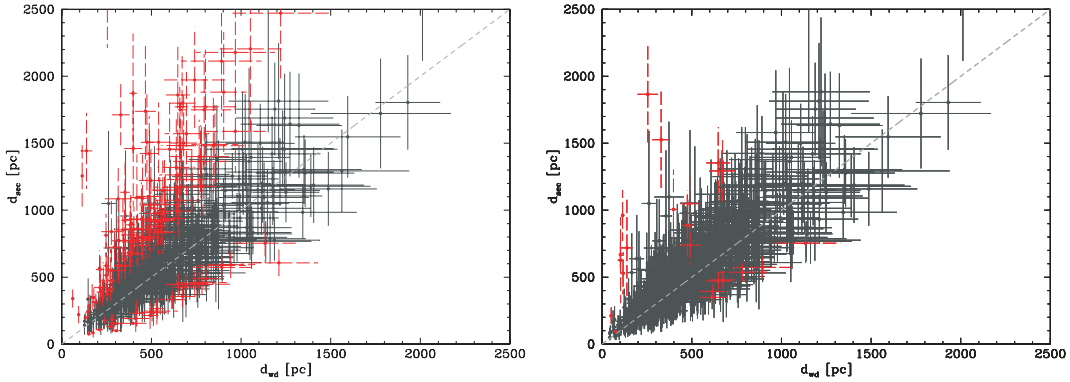

Figure 11. Left-hand panel: comparison of $d_{\rm sec}$ and $d_{\rm wd}$ obtained from our spectral decomposition and white-dwarf fits to the SDSS spectra. Approximately one-fifth of the systems are $d_{\rm sec} > d_{\rm wd}$ outliers by more than 1.5σ (red dots). Right-hand panel: the spectral types of the secondary stars were adjusted by one to two spectral classes to achieve $d_{\rm wd} = d_{\rm sec}$.

6.4 Distances

In Section 5, we derived two independent distance estimates for the WDMS binaries in our catalogue. We compare these values in Fig. 11. Here we only consider systems with relative errors of less than 25 per cent in the white-dwarf distance. The relative error in $d_{\rm sec}$ is dominated by the scatter in the spectral-type–radius relation provided in Rebassa-Mansergas et al. (2007). Hence, it represents an intrinsic uncertainty rather than a statistical error related to the fit and we therefore do not apply any cut in $d_{\rm sec}$. Moreover, we excluded from the analysis any WDMS binary containing a white dwarf of less than 12 000 K, as spectral fits tend to overestimate the surface gravity and hence the mass (Koester et al. 2009), leading to an underestimate of the white-dwarf radius and hence the distance. If more than one SDSS spectrum is available, we use averaged distances. This procedure resulted in a sample of 603 WDMS binaries.

In the top panel of Fig. 11, black dots represent systems in which the two distances agree within 1.5σ (approximately three-fourth of the total sample) level, while the differences in the two distances obtained for the objects in red exceed this limit. Most of the $\geq 1.5\sigma$ outliers are above $d_{\rm sec} = d_{\rm wd}$ (approximately one-fifth of our WDMS binaries), while we find $d_{\rm sec} < d_{\rm wd}$ for only $\sim$5 per cent of the entire sample. Hence, there seems to be a systematic effect that leads to overestimating the secondary star distances. As in Rebassa-Mansergas et al. (2007), we assume that magnetic activity raises the temperature of the inter-spot regions in active stars that are heavily covered by cool spots, leading to a blueshift of the optical colours compared to inactive stars. However, to finally evaluate this interpretation one needs to perform a detailed activity analysis of our sample based on Hα emission. This would further require to distinguish between the different sub-samples forming the WDMS binary population, i.e. PCEBs and wide systems, as the fraction of active stars is expected to depend on the rotation rate. This is beyond the scope of this paper but will be presented in a forthcoming publication.

As a first simple test, we adjust the spectral type of the secondaries to bring into agreement the two distances. It turns out that a change of one to two spectral subclasses is enough for the majority of cases. Only 10 systems in the right-hand panel of Fig. 11 need a change of more than two spectral subclasses to reach $d_{\rm sec} = d_{\rm wd}$. We have inspected these objects in more detail and the large discrepancy might be explained as follows.

(i) Six objects contain hot white dwarfs, i.e. SDSS J003221.86+073934.4, SDSS J032510.84−011114.1, SDSS J080229.99+072858.1, SDSS J095719.25+234240.8, SDSS J101323.90+043946.1, SDSS J141536.40+011718.2. If these are short orbital period systems, irradiation of the secondary by the hot primary may lead to overestimating the distance to the secondary star. These WDMS binaries might therefore be considered as candidates to probe for radial velocity variations. SDSS J032510.84−011114.1 benefits from two SDSS J radial velocity measurements in Table 9, but no variation is detected. This may reflect the speculative nature of the just given argument or be caused by the SDSS spectroscopy sampling the same orbital phase twice.

(ii) Three systems (SDSS J025306.37+001329.2, SDSS J204729.04−064536.7, SDSS J210624.12+004030.2) are resolved in their SDSS images. Depending on the exact placement of the fibre, the flux contribution of one or both stars is likely to be underestimated. This translates to underestimated flux scaling factors and overestimated distances.

(iii) For one object, SDSS J232624.72−011327.2, the S/N of the corresponding SDSS spectrum is very low (S/N = 4.2). This is probably the reason for the discrepancy found in the distances.

7 COMPARISON WITH PREVIOUS STUDIES

Since Smolčić et al. (2004) discovered the WDMS binary bridge several SDSS WDMS binary catalogues have been presented, and several fitting routines to determine the stellar parameters have been applied. In this section, we compare in more detail the results of our spectral decomposition method with those obtained by earlier studies.

7.1 Comparison with Rebassa-Mansergas et al. (2007)

Given that the SDSS spectra reduction pipeline was improved with DR6 (Adelman-McCarthy et al. 2008), we decided to compare the stellar parameters obtained here with those we obtained in Rebassa-Mansergas et al. (2007). The stellar parameters for those objects with multiple SDSS spectra were averaged. Fig. 12 compares white-dwarf effective temperatures, surface gravities and secondary spectral types. Both studies agree within the errors in the majority of cases, with average relative differences of 13.5 and 2.5 per cent in $T_{\rm eff}$ and $\log g$, respectively, and an average difference of 0.3 spectral subtypes. We obtain significantly different values especially for

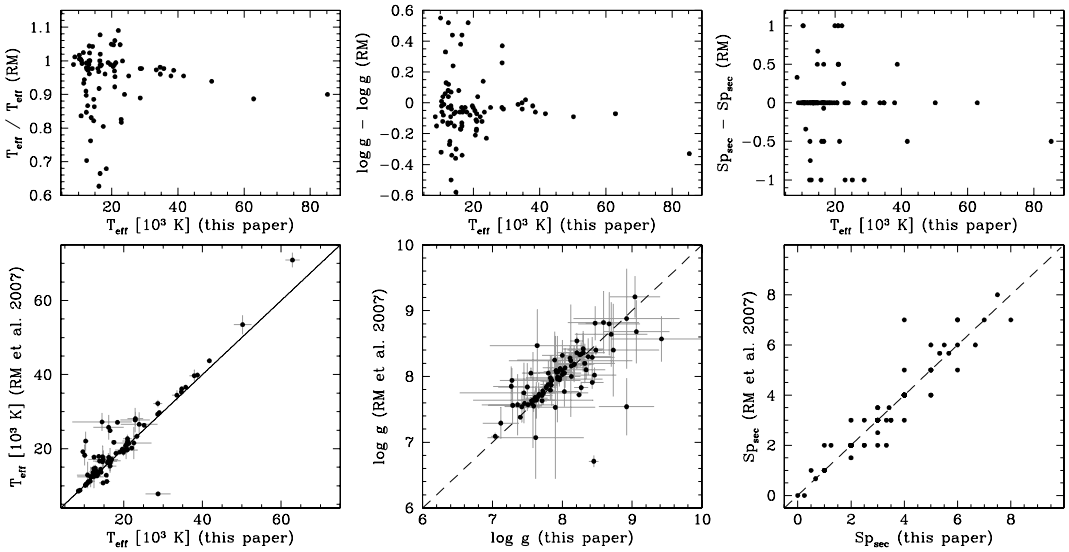

Figure 12. Bottom panels from left to right: comparison of the white-dwarf effective temperatures, surface gravities and the spectral types of the secondary stars determined in this work and those of Rebassa-Mansergas et al. (2007). Top panels, from left to right: the white-dwarf effective temperature ratio, and the difference in surface gravity and the secondary's spectral types from the two studies as a function of the white-dwarf temperature.

systems containing white dwarfs with temperatures in the range of 10 000–20 000 K (see the top panels of Fig. 12). In ∼50 per cent of the cases, this is due to the fact that we are making use of ultraviolet *GALEX* magnitudes to constrain the white-dwarf line fit solutions in this paper (see Section 5). In the remaining ∼50 per cent cases, this is most likely a consequence of the systematic changes in the flux calibration pipeline. The most dramatic case is SDSS J151045.70+404827, a clear outlier in the bottom left-hand panel of Fig. 12, with a difference in $T_{\rm eff}$ and log g of 21 000 K and 1.7 dex, respectively. This was one of the cases in which the solution was modified by the use of *GALEX* magnitudes. The obtained differences in spectral type are consistent with the general uncertainty of our decomposition/fitting procedure of 0.5 spectral subclasses (see Section 5). Only for SDSS J173548.36+541424.4 does this difference exceed one spectral subtype. This system is very faint ($i \sim 20$), and the low S/N causes the spectral-type determination to be rather uncertain.

7.2 Comparison with van den Besselaar et al. (2005)

We have identified in this work 53 DB/M dwarf binaries, 13 of them in common with van den Besselaar et al. (2005). The stellar parameters of these systems are given in Table 8. Apparently, the white-dwarf temperatures differ significantly. As van den Besselaar et al. (2005) used DR3 SDSS spectra and measured all parameters by assuming a white-dwarf mass of 0.6 $M_{\odot}$, these discrepancies are not too surprising. In addition, as stated by van den Besselaar et al. (2005), their derived effective temperature is related to the fitting of the secondary star, i.e. changing the spectral type by one subclass can lead to differences in the white-dwarf effective temperatures of 8000 to 10 000 K.

The distance measurements by van den Besselaar et al. (2005) are based on the white-dwarf fitting, while we use the secondary star spectral type in case the primary is not a DA white dwarf. Taking into account the uncertainties involved in both distance measurements, we obtain reasonable agreement between both values.

Concerning the spectral type of the companion stars, our values are in good agreement with those obtained by van den Besselaar et al. (2005). In all but two (SDSS J093645.14+420625.6 and SDSS J113609.59+484318.9) cases, the difference does not exceed one subclass. SDSS J093645.14+420625.6 is an $i = 20$th magnitude object with a low S/N spectrum leading to large uncertainties in the obtained parameters. SDSS J113609.59+484318.9 contains a hot white dwarf ($\gtrsim$30 000 K) that significantly contaminates the spectrum of the M-dwarf.

Table 8. Effective temperatures, spectral types and distances obtained from van den Besselaar et al. (2005) and this work. The first line on each systems corresponds to the results obtained by van den Besselaar et al. (2005) and the second line provides our results.

SDSS J	$T_{\rm eff}$ (K)	err	Sp	d (pc)	err
075235.79+401339.0	30 252	4000	3	1544	
	16 811	56	3	1295	255
080636.85+251912.1	24 266	4000	3	1045	
	17 439	78	3	852	168
093645.14+420625.6	15 919	4000	5	860	
	–	–	3	1949	384
100636.39+563346.8	14 575	4000	4	531	
	16 071	46	3	817	161
102131.55+511622.9	30 252	4000	4	700	
	17 622	25	5	479	245
113609.59+484318.9	38 211	4000	6	354	
	31 324	234	3	896	176
134135.23+612128.7	30 694	4000	3	1054	
	16 051	10	3	886	175
143222.06+611231.1	36 815	4000	3	879	
	16 180	47	4	527	155
144258.47+001031.5	30 694	4000	3	674	
	31 324	234	4	358	105
150118.40+042232.3	26 020	4000	3	1220	
	18 394	40	3	1111	219
162329.50+355427.2	24 266	4000	3	695	
	15 730	39	3	579	114
220313.29+113236.0	30 694	4000	4	1085	
	19 992	127	4	1036	305
232438.31−093106.5	36 815	4000	3	911	
	19 340	96	4	530	156

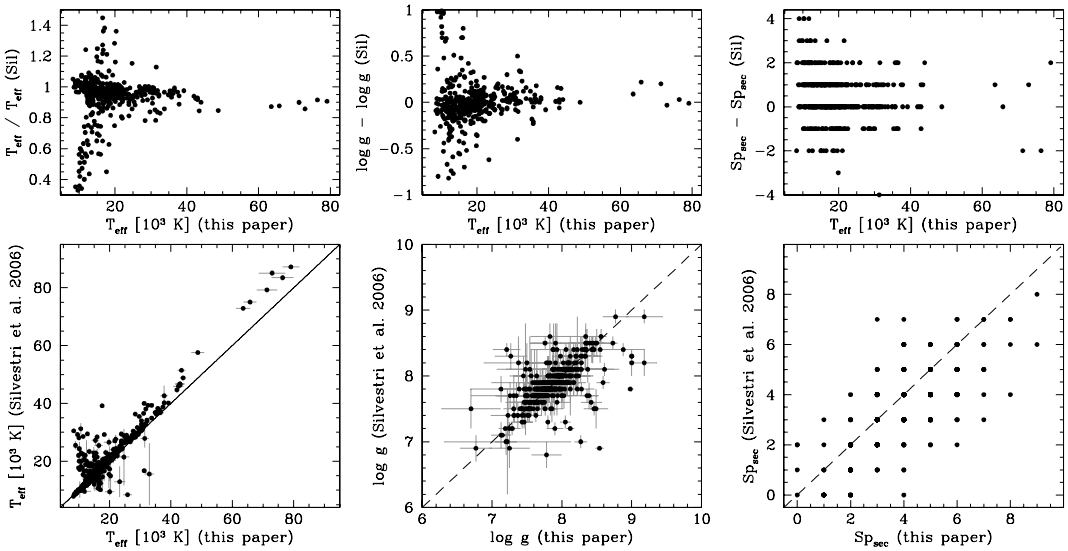

Figure 13. Bottom panels from left to right: comparison of the white-dwarf effective temperatures and surface gravities and the spectral types of the secondary stars determined from our fits and those of Silvestri et al. (2006). Top panels, from left to right: the white-dwarf effective temperature ratio, and the difference in surface gravity and the secondary's spectral types from the two studies as a function of the white-dwarf temperature.

7.3 Comparison with Silvestri et al. (2006)

We compare in Fig. 13 the white-dwarf effective temperatures and surface gravities, and secondary spectral types obtained in Section 5 with those obtained by Silvestri et al. (2006). We considered a sample of 421 spectra for which both studies present values for the stellar parameters.

The average relative difference in effective temperatures and surface gravities is reasonably low, i.e. 14.7 and 2 per cent, respectively. For systems with white-dwarf temperatures below ∼20 000 K, however, the values obtained can differ by up to 22 100 K and 1.6 dex. As discussed in Rebassa-Mansergas et al. (2007), we interpret this strong disagreement to be caused by the ambiguity between the hot and the cold solutions. At higher temperatures (>50 000 K), our fits tend to provide lower values of $T_{\rm eff}$ than those given in Silvestri et al. (2006). This is probably caused by their use of DR4 spectra that were reduced with a different pipeline. In the majority of cases, the secondary star spectral types are in reasonably good agreement (i.e. the difference is not exceeding one subtype). However, for ∼17 per cent of the WDMS binaries the difference is of two or more subtypes, with a maximum difference of 4.

We have also inspected the systems that Silvestri et al. (2006) failed to fit and found that in ∼70 per cent of these, we are able to find a solution. As previously discussed in Rebassa-Mansergas et al. (2007), this indicates that our method is more robust if the S/N is low or if one of the stellar components contributes little to the total flux.

7.4 Comparison with Heller et al. (2009)

Heller et al. (2009) studied a sample of 857 WDMS binary candidates. For 636 of these systems, they provide the results of an independent spectroscopic parameter fitting method. Figure 14 compares the white-dwarf effective temperatures, distances and surface gravities obtained by Heller et al. (2009) with the values obtained here. The average relative differences between the two analysis are 12.1 per cent (white-dwarf temperature), 23.9 per cent (distance) and 3.6 per cent (surface gravity).

Fig. 15 compares the effective temperatures, distances and masses of the secondary stars in both data sets. In this case, the average relative differences are 3.5 per cent (effective temperature), 42.1 per cent (distance) and 42 per cent (mass). While we used M star templates in our fitting, Heller et al. (2009) used a grid of PHOENIX model spectra (Hauschildt & Baron 1999). The colours refer to objects containing secondaries of the same spectral type, i.e. red, blue, green, yellow, magenta, black and cyan for spectral types M1–M7. Values of effective temperatures and masses for the systems in our catalogue were estimated using the spectral-type–radius–mass–effective temperature relations given in Rebassa-Mansergas et al. (2007). Therefore, WDMS binaries containing secondaries of the same spectral type are associated with the same effective temperature and mass, while the estimates provided by Heller et al. (2009) cover a considerably larger range in both mass and effective temperature (lower left-hand and lower right-hand panels of Fig. 15). According to the lower right-hand panel, Heller et al. (2009) measure systematically lower masses. A comparison of the distances obtained to the secondary stars is shown in the middle panels of Fig. 15. Since the observed flux is the same for a given SDSS spectrum, the only difference between both methods comes from the radius and the flux at the stellar surface. As the grid of model spectra is not finer than our grid of template spectra, both methods differ by a constant for a given spectral-type/secondary mass combination. This can clearly be seen in the bottom middle panel of Fig. 15: for each pair of template/model spectrum, we obtain one or two straight lines in the distance–distance diagram. It seems that we overestimate and/or Heller et al. (2009) underestimate the distances. However, we presented in Rebassa-Mansergas et al. (2007) (see also Section 6.4) a reasonable explanation for approximately one-fifth of the WDMS binaries with $d_{\rm sec} > d_{\rm wd}$, while there is no obvious physical mechanism that may account for the estimated white-dwarf distances being systematically smaller than the companion distances as the values of Heller et al. (2009) seem to suggest. We have to keep this in mind though the uncertainties

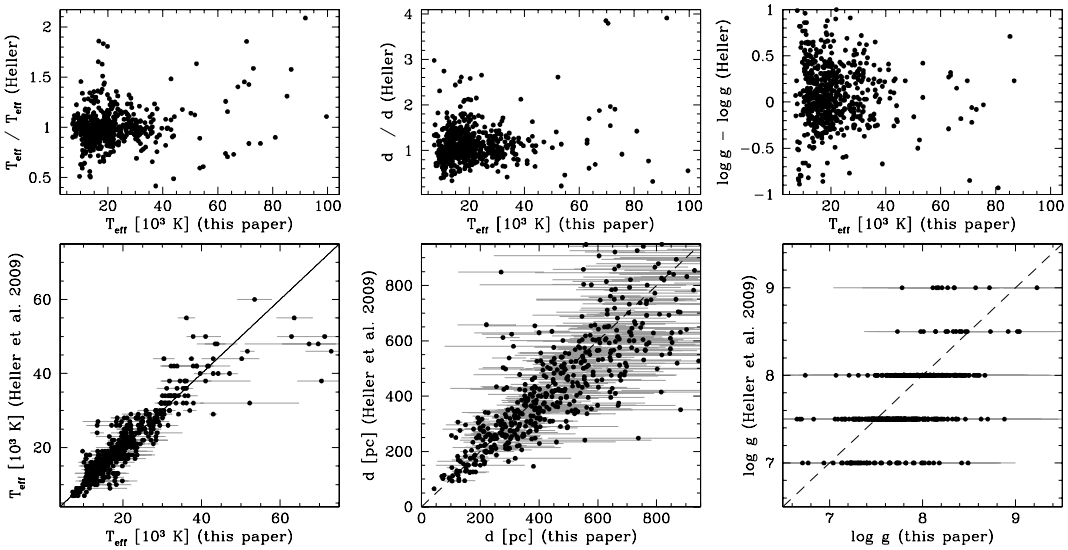

Figure 14. Bottom panels from left to right: comparison of the white-dwarf effective temperatures, distances and surface gravities determined from our fits and those of Heller et al. (2009). Top panels, from left to right: the white-dwarf effective temperature and distance ratios, and the difference in surface gravity from the two studies as a function of the white-dwarf temperature.

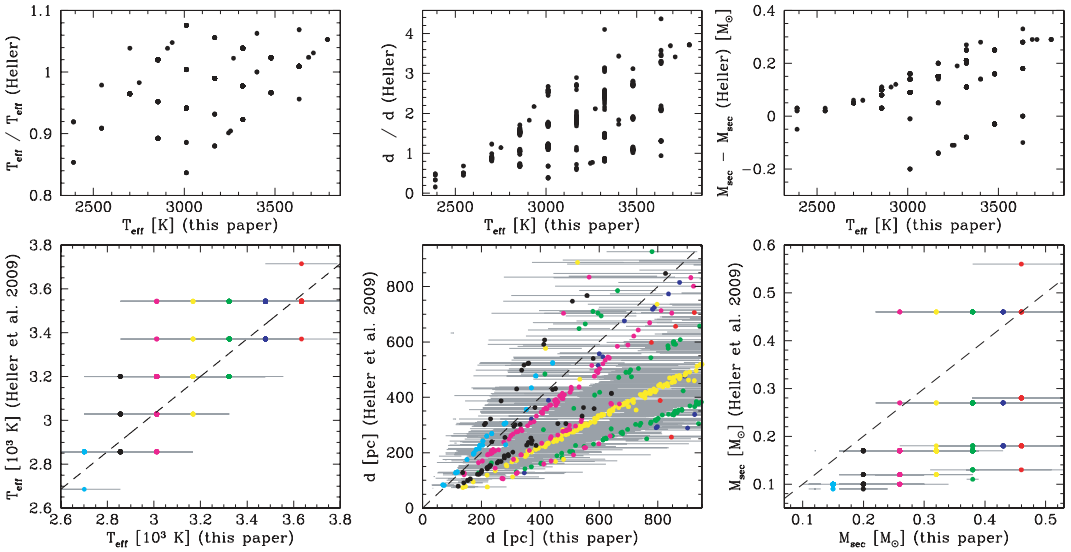

Figure 15. Bottom panels from left to right: comparison of the secondary star effective temperatures, distances and masses determined from our fits and those of Heller et al. (2009). The colours red, blue, green, yellow, magenta, black and cyan refer to spectral types M1–M7, respectively. Top panels, from left to right: the secondary star effective temperature and distance ratios, and the mass difference from the two studies as a function of the white-dwarf temperature.

related to both methods are quite large and the activity interpretation of the systematically larger secondary distances still needs to be confirmed. We therefore conclude that the question of whether our templates or the model spectra provide more reliable distances remains open.

8 SELECTION EFFECTS

In Rebassa-Mansergas et al. (2007), we briefly discussed possible selection effects that may affect the observed SDSS WDMS binary population. The much larger sample presented here allows us to investigate these selection effects in more detail. To avoid contaminations from unreliable stellar parameters, we base our analysis on systems with mean relative errors of less than 25 per cent in their white-dwarf parameters. As discussed in detail in Rebassa-Mansergas et al. (2007), the distances derived from the white-dwarf parameters are probably more reliable than those derived from the secondary stars. We therefore use the white-dwarf distances here and quote them simply as distances in the following.

Fig. 16 shows three density maps that illustrate the selection effects affecting the SDSS WDMS sample. Due to the restrictions in the white-dwarf parameters 597, 692 and 1052 systems (from top to bottom) were considered. The $\log T_{\rm eff}$, $d_{\rm wd}$ density map in the top panel shows that binaries with white-dwarf primaries cooler than 10 000 K are only detectable at relatively short distances ($d \lesssim$ 400 pc), while systems containing hotter white dwarfs have been detected at a much wider range of distances (∼200–1000 pc). In addition, there is obviously a general trend of increasing distance with white-dwarf temperature. This is straightforward to understand as cold white dwarfs become too faint to be detected at larger

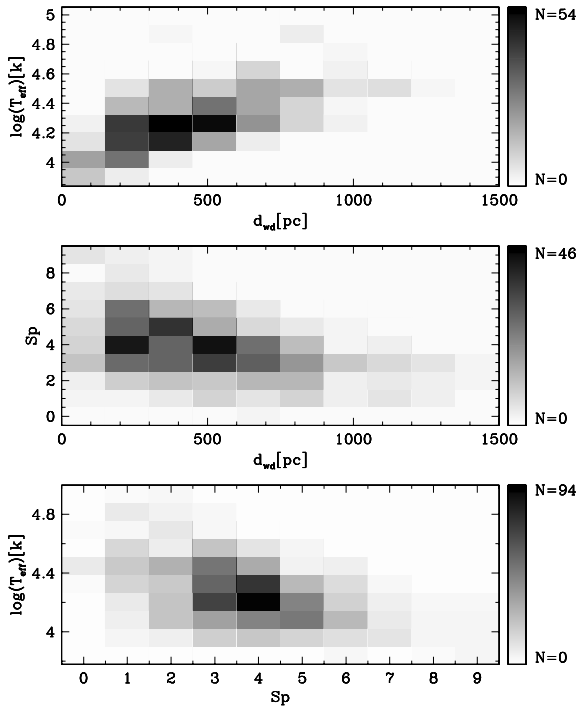

Figure 16. Selection effects in SDSS WDMS binaries can be understood by analysing the density maps obtained from their stellar parameters. From top to bottom: the (log $T_{\rm eff}$, $d_{\rm wd}$), ($d_{\rm wd}$, Sp) and (log $T_{\rm eff}$, Sp) density maps.

distances. In contrast hot white dwarfs are intrinsically brighter, but also rarer than cold white dwarfs, and hence dominate at larger distances where the volume surveyed by the SDSS is sufficiently large. Most objects are hence concentrated at ∼400-500 pc, with white-dwarf effective temperatures between ∼15 000 and 25 000 K, as also shown in the effective temperature distribution (Fig. 9). The middle panel of Fig. 16 shows a similar effect but for the secondary star spectral types, Sp. Early M-dwarfs are relatively hot and consequently exceed the lower SDSS brightness limit at distances of $\lesssim$300 pc. In contrast, late-type secondaries are cold enough to be detected at short distances (∼100–200 pc) but too dim to be observed at distances larger than ∼500 pc. Finally, the bottom panel of Fig. 16 shows the log $T_{\rm eff}$, Sp density map. A clear trend of later spectral-type companions to colder white-dwarf primaries can be seen. This is again easy to understand: while late-type companions to hot white dwarfs are too faint to be detected, cold white-dwarf primaries are outshined by early spectral-type secondaries.

The selection effects just described can explain the cut-off at early spectral types in the bottom panel of Fig. 9, as the white-dwarf primaries are not detectable. The scarcity of systems with later-type (>M6) secondaries, however, is probably not only related to selections effects, as the spectral-type distribution of low-mass field stars also peaks at Sp $\simeq$ M4–M5 and decline towards later spectral types (e.g. Farihi et al. 2005; Reid, Cruz & Allen 2007; Reid et al. 2008). The lack of WDMS binaries with late-type companions is therefore probably an intrinsic property of the WDMS binary population that appears more pronounced due to selection effects. We will address this systematically in a forthcoming publication.

From the analysis of Fig. 16, we conclude that a 'typical' SDSS WDMS binary contains an M3–M4 companion, an ∼10 000–20 000 K primary and is observed at a distance of ∼400–500 pc. However, we have to keep in mind that a typical SDSS WDMS binary is not necessarily a typical WDMS binary. Overcoming the selection effects just described requires to combine the SDSS with complementary magnitude-limited surveys. Detecting binaries consisting of a hot white-dwarf and a late-type companion is most likely to arise from the use of infrared surveys such us UKIDSS or Two-Micron All-Sky Survey (2MASS), while the identification of cool white dwarfs with early-type-dominated M-dwarfs requires to incorporate ultraviolet surveys such as *GALEX* (Maxted et al. 2009).

9 COLOUR–COLOUR DIAGRAMS

We have provided in the previous sections of this paper a detailed spectroscopic analysis of WDMS binaries in the SDSS. In this section, we make use of the photometric magnitudes given in Table 5 and combine them with the stellar parameters measured from the SDSS spectra to investigate the appearance of WDMS binaries in colour–colour space. Figs 17 and 18 show four relevant colour–colour diagrams. Stellar sources are shown in grey, DA/M WDMS binaries in yellow, the few DB/M in blue and the DC/M binaries in green. Finally, DA–DB–DC/K systems are shown in red, while the black dots represent the WD/M-K binaries (see Section 2.4). A general feature evident in all diagrams is that a certain number of systems appear to be outliers from the general stellar locus of WDMS binaries, i.e. the WDMS binary bridge first described in Smolčić et al. (2004). We have inspected these outliers and find the majority of them being resolved in the SDSS images (see Section 2.3).

To further evaluate the information provided by photometry we show the white-dwarf effective temperature and secondary star spectral-type distributions in six different regions for each colour–colour diagram, as indicated by the horizontal (dotted) and vertical (dashed) lines. The resulting distributions are shown above and below the colour–colour diagrams. As previously, we considered only those white-dwarf effective temperatures with relative error less than 25 per cent. In the following subsections, we briefly describe the main conclusions that can be drawn from the four colour–colour diagrams.

9.1 $u - g$ versus $g - r$

The most commonly used SDSS colour–colour diagram for stellar sources in the SDSS is $u - g$ versus $g - r$ (Fan 1999; Richards et al. 2002; Schreiber et al. 2007). Inspecting the left-hand side of Fig. 17, it can be clearly seen that the white-dwarf effective temperature distribution is shifted towards lower temperatures if $u - g$ or $g - r$ increases, i.e. for redder colours (compare the left, centre and right as well as the top and the middle distributions). Only two WDMS binaries with reliable effective temperatures are found in the bottom region close to the main sequence. As expected, the distributions of secondary spectral types contain more early-type secondaries if one moves to redder colours (left to right or top to bottom).

9.2 $nuv - u$ versus $u - r$

The $nuv - u$ versus $u - r$ colour–colour diagram is provided in the middle right-hand panel of Fig. 17. The white-dwarf effective temperature and spectral-type distributions in the six regions of the diagram (see top and bottom right-hand panels in Fig. 17) are similar to those discussed in the above subsection, the main difference being

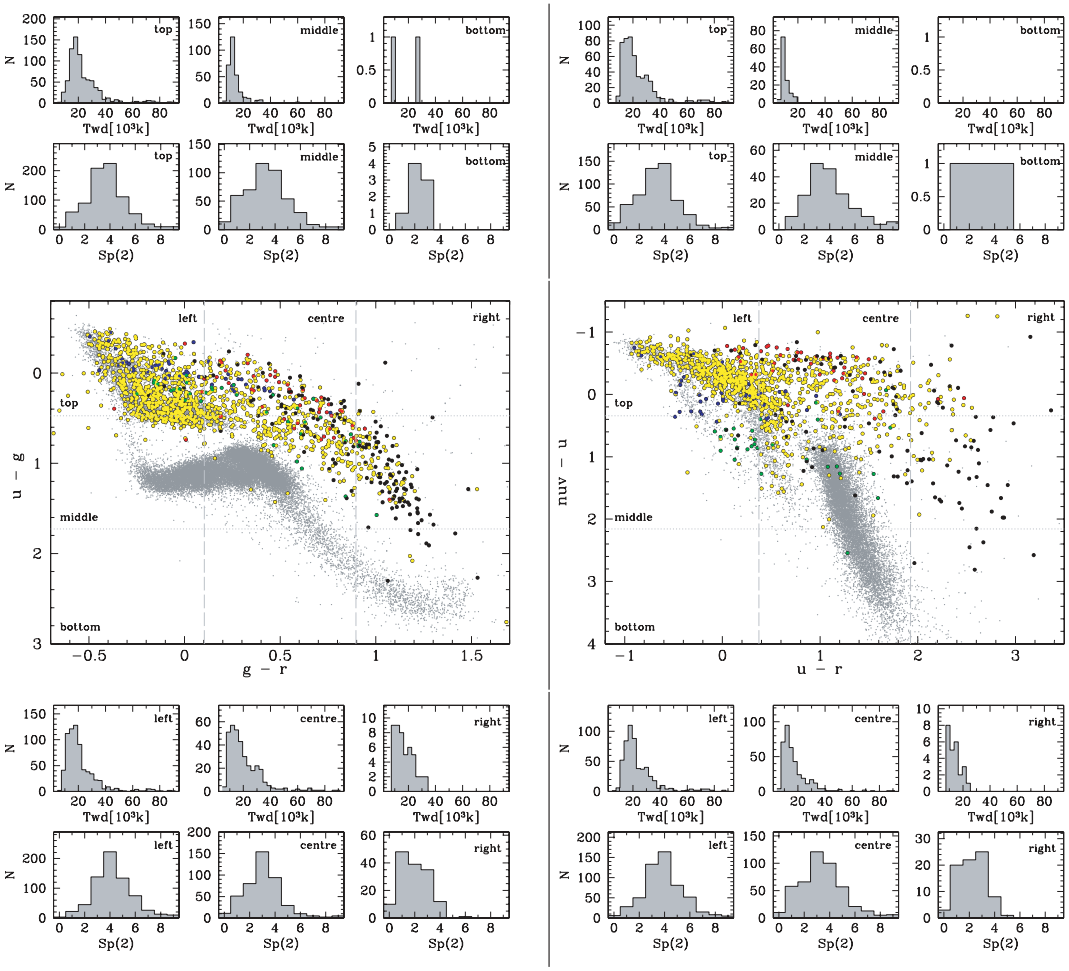

Figure 17. Middle left: $u - g$ versus $g - r$ colour–colour diagram. WDMS binaries are represented according to their binary components as follows: DA/M binaries in yellow, DB/M in blue, DC/M in green, DA–DB–DC/K in red and WD/M in black. Stellar sources are represented with grey dots. Two vertical (dashed) lines divide the diagram in three rectangular regions (columns left, centre, right). In the same way, two horizontal (dotted) lines divide the diagram into three different regions (rows top, middle, bottom). Top and bottom left: distributions of white-dwarf effective temperature and spectral type of the companions obtained for the six different regions outlined above (three rows and three columns). The right-hand panels follow the same structure, but for the $nuv - u$ versus $u - r$ colour–colour diagram.

the decrease in the number of systems. This is due to the smaller percentage of SDSS WDMS binaries that have been detected with *GALEX*.

9.3 $nuv - i$ versus $nuv - H$

Figure 18 (left-hand panels) shows the $nuv - i$ versus $nuv - H$ colour–colour diagram and the corresponding distributions of white-dwarf effective temperatures and secondary spectral types. Clearly, using SDSS–*GALEX*–UKIDSS magnitudes reduces the number of WDMS binaries and the distributions shown are statistically less robust. However, the general trend observed in the previous colour–colour diagrams remains: systems composed of white dwarfs hotter than 20 000 K are generally detected in the top and left regions of the diagram and there is a clear trend of decreasing white-dwarf effective temperature towards redder colours (top to bottom and left to right). The previously observed shift towards earlier spectral types for redder colours still seems to be present, but is much less pronounced. The most striking feature of the colour–colour diagram is the nice separation of WDMS binaries and single stars.

9.4 $i - J$ versus $J - H$

Finally, we provide in Fig. 18 (right-hand panels) the $i - J$ versus $J - H$ red colour–colour diagram and the corresponding distributions. Again, due to the reduced number of systems the overall trend of having less hot white dwarfs and more early spectral-type secondaries for redder colours seems to be present but less significant. Nearly all systems containing hot white dwarfs are located in the upper region. This colour–colour diagram represents an additional example of nicely separating WDMS binaries and single stars. We provide several colour cuts that can be used to select WDMS binaries in the next section.

10 COLOUR CUTS

Having studied in the previous section the relation between colours and stellar parameters (i.e. white-dwarf effective temperature and spectral type) in four colour–colour space diagrams, we define here four colour cuts of WDMS binaries. The fact that we are considering a total of 11 photometric bandpasses (two from *GALEX*, five from the SDSS and four from the UKIDSS) increases considerably the number of possible colour-cut selections. We here provide four

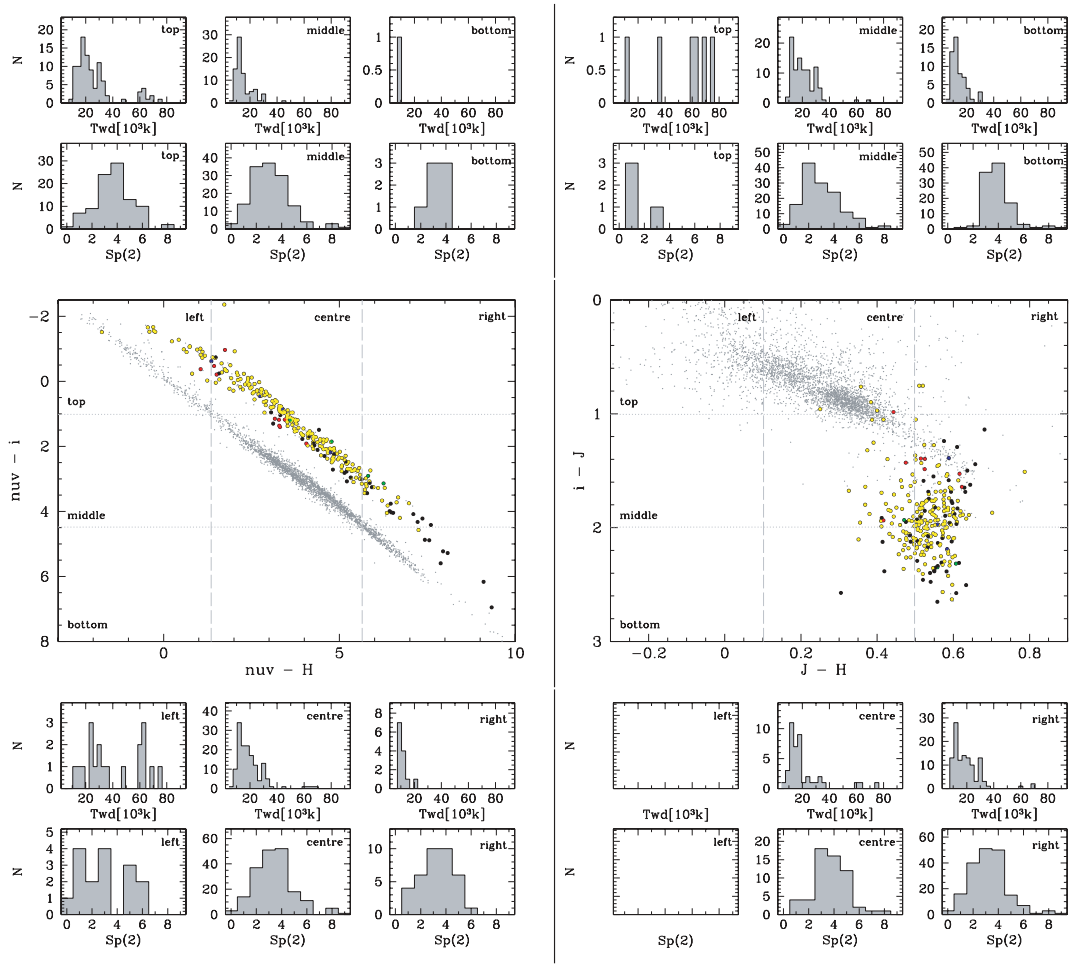

Figure 18. Same as in Fig. 17 but for the $nuv - i$ versus $nuv - H$ (left) and $i - J$ versus $J - H$ (right) colour–colour diagrams.

examples (two of them already introduced in Section 9) in which WDMS binaries are clearly separated from the locus of single main-sequence stars (see Fig. 19). To quantify how complete these colour cuts are would imply an analysis on the different SDSS-I, SEGUE, Stripe 82 areas, where different target strategies were tested. Such an endeavour is beyond the scope of this paper and will be pursued elsewhere.

The top left-hand panel of Fig. 19 shows the $nuv - i$ versus $nuv - H$ colour–colour diagram introduced above, which offers an excellent opportunity to unambiguously isolate WDMS binaries from single main-sequence stars and white dwarfs with a simple colour cut. We represent in light grey main-sequence stars and white dwarfs, and in dark grey WDMS binaries. With a straight black line, i.e.

$$(nuv - i) < -0.85 + 0.83 \times (nuv - H), \quad (2)$$

both populations can be distinguished.

As we have seen in Section 9, WDMS binaries and single stars also separate nicely in the $i - J$ versus $J - H$ colour plane. However, the location of WDMS binaries containing hot white dwarfs overlaps with those of single stars. The colour cuts shown in the top right-hand panel of Fig. 19, i.e.

$$0.3 < (J - H) < 0.7, \quad (3)$$

$$(i - J) > 1.2, \quad (4)$$

$$(z - J) > 0.4 + 1.85 \times (J - H), \quad (5)$$

will therefore mainly select WDMS binaries composed of cold white dwarfs.

Recently, Bianchi et al. (2007) studied the properties of the *GALEX*–SDSS matched source catalogues and classified sources by studying their colours. Inspired by their fig. 5, in the bottom left-hand panel of Fig. 19 we show the $fuv - nuv$ versus $r - z$ colour diagram and provide colour cuts that should select the main population of WDMS binaries:

$$(r - z) > -0.3, \quad (6)$$

$$(fuv - nuv) < 0.85 + 3.9 \times (r - z). \quad (7)$$

Finally, we provide in the bottom right-hand panel of Fig. 19 the colour–colour diagram and colour cuts for WDMS binaries in $y - K$ versus $u - z$. Again, stars are represented in light grey, WDMS binaries in dark grey and colour cuts by straight black lines. This colour diagram has been already used by Chiu et al. (2007) for quasar selection. Here, we only slightly modified their colour cuts and obtain

$$(u - z) > 5, \quad (8)$$

$$(y - K) > 0.7, \quad (9)$$

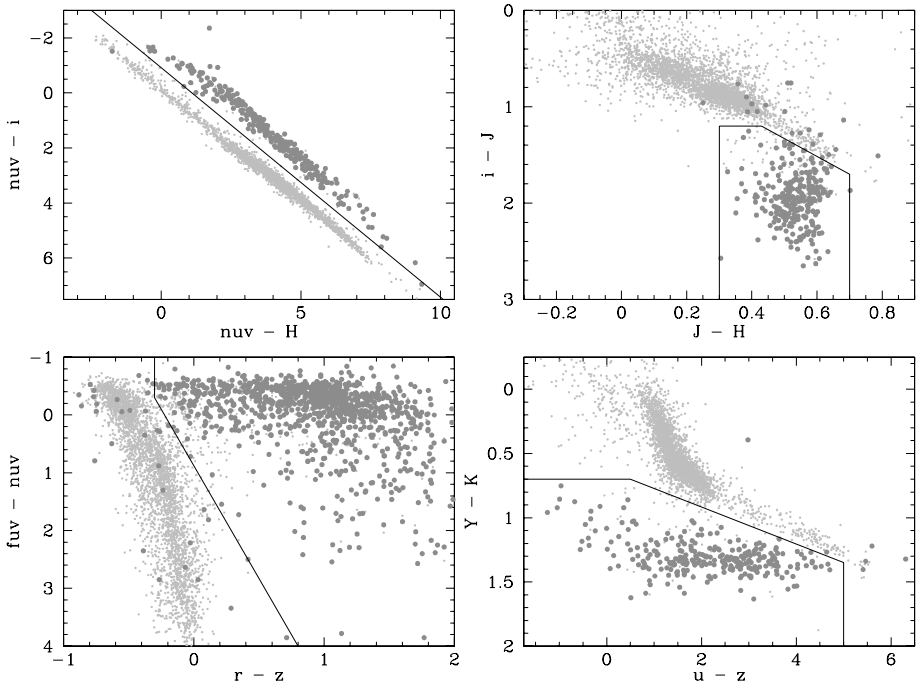

Figure 19. Colour-cut selection for WDMS binaries in $nuv - i$ versus $nuv - H$ (top left), $i - J$ versus $J - H$ (top right), $fuv - nuv$ versus $r - z$ (bottom left) and $y - K$ versus $u - z$ (bottom right). Main-sequence stars and white dwarfs are represented in light grey, WDMS binaries in dark grey and colour cuts by black straight lines.

Table 9. Radial velocities measured from the Na I λλ8183.27, 8194.81 doublet and the Hα emission for 1068 systems in our catalogue. The complete table can be found in the electronic version of the paper (see Supporting Information). In the last column, we quote with 'y' and 'n' those radial velocity values obtained from spectra that are and that are not combined from individual exposures taken on different nights, respectively. We use '–' to indicate that no radial velocity is available.

SDSS J	HJD 245	RV (Na) (km s^{-1})	err	RV (Hα) (km s^{-1})	err	Com.?
000152.09+000644.7	1791.8092	0.7	21.1	24.2	16.7	n
001247.18+001048.7	2519.8962	–	–	12.3	18.6	n
001247.18+001048.7	2518.9219	−14.3	30.1	30.6	14.4	n
001359.39-110838.6	2138.3933	28.9	16.9	–	–	y
001726.64–002451.2	2559.7852	−33.7	15.5	−30.1	11.4	n
001726.64–002451.2	2518.9219	−19.8	17.8	−26.5	11.8	n
001733.59+004030.4	1794.7737	−3.7	15.8	–	–	n
001749.25–000955.4	2518.9218	−18.3	17.4	−3.2	11.6	n
001749.25–000955.4	1794.7737	−36.6	15.5	−22.8	10.1	n
001855.20+002134.5	1816.8000	41.4	27.4	–	–	n
001855.20+002134.5	1893.0883	15.0	22.2	–	–	y
002143.78–001507.9	2581.7411	1.5	14.7	–	–	n
002157.91–110331.6	3318.6951	148.4	15.8	−9.1	13.3	y
–	–	–	–	–	–	–

$$(y - K) > 0.6 + 0.14 \times (u - z), \quad (10)$$

which should successfully select WDMS binaries.

11 RADIAL VELOCITIES AND NEW PCEB CANDIDATES

In this section of the paper we follow Rebassa-Mansergas et al. (2007) and use the Na I λλ8183.27, 8194.81 absorption doublet and/or the Hα emission to measure radial velocities. As in Rebassa-Mansergas et al. (2008) and Schreiber et al. (2008), we use a single width parameter for both line components in the Na I doublet. The radial velocities of 1068 systems with the pronounced Na I λλ8183.27, 8194.81 absorption doublet and/or Hα emission in their SDSS spectra are given in Table 9, where we also include the HJD of the observations.[2] As discussed in Rebassa-Mansergas et al. (2007), a significant fraction of SDSS spectra is combined from

[2]Note that the HJDs in Rebassa-Mansergas et al. (2007) were wrong by −0.5 d because of an erroneous conversion of the FITS headers of the SDSS spectra.

Table 10. Upper limits to the orbital periods of the five PCEB candidates identified in Section 11. White-dwarf masses are taken from Table 7 except for SDSS J2346+4340, where we assume of mass of 0.5 $M_{\odot}$ (see Fig. 9). Secondary star masses are estimated from Table 5 in Rebassa-Mansergas et al. (2007). K_{sec} values are obtained from Table 9, where we use the Na I doublet radial velocities for SDSS J2346+4340.

SDSS J	0333[a] +0054	0743 +2835	1453 +0055	2318 +0034	2346 +4340
P_{orb} (d)	575	121	8	5	2

[a]The effective temperature is below 12 000 K, and consequently the white-dwarf mass is likely overestimated.

observations that have been taken in different nights which leads to a reduced sensitivity to radial velocity variations. We indicate this in the last column of Table 9.

A comparison with the radial velocities obtained in Rebassa-Mansergas et al. (2007) gives an average relative difference of 19.5 per cent, and the measurements generally overlap within the errors. The reasons for the small changes have been already discussed in detail in Rebassa-Mansergas et al. (2008) and can be summarized as follows: (1) we modified the procedure to fit the Na I absorption doublet by using a single width parameter for both line components and (2) we used DR6 spectra here (instead of DR5).

As described in Section 1, the orbital period distribution of WDMS binaries is expected to be bimodal, separating long orbital period systems whose stellar components evolve like single stars from short orbital period systems that suffered from mass transfer interactions, mostly CE evolution (Willems & Kolb 2004). As demonstrated by Rebassa-Mansergas et al. (2007), multiple SDSS spectroscopy of WDMS binaries can be used to measure radial velocity variations thereby eventually identifying candidates for being a PCEB. Our criterion for calling a WDMS binary a strong PCEB candidate is radial velocity variations with 3σ significance. This is evaluated by calculating the χ^2 of the measured radial velocities against their mean value. The incomplete γ function then gives the probability for the measured radial velocities being consistent with a constant value. If this probability is below 0.0027 the measured radial velocity variations are 3σ significant, and we consider the corresponding WDMS binary a strong PCEB candidate.

Here we find nine and 16 PCEB candidates using the Na I doublet and Hα emission, respectively. A comparison with the results obtained in Rebassa-Mansergas et al. (2007) shows that four systems, i.e. SDSS J030904.82−010100.9, SDSS J113800.35−001144.5, SDSS J173727.27+540352.2 and SDSS J234534.50−001453.7, are no longer considered PCEBs while we find five new PCEB candidates, namely SDSS J033301.51+005418.5, SDSS J074329.62+283528.0, SDSS J145300.99+005557.1 SDSS J231874.73+003403.3 and SDSS J234638.76+434041.7, respectively. Apparently, the differences in the method of determining radial velocities and/or the re-reduction of the SDSS data can cause a given system to move either way across our criterion (Rebassa-Mansergas et al. 2008). The Na I absorption lines from the secondary star are a more robust probe for radial velocity variations, and we consequently consider that additional follow-up spectroscopy is necessary for those PCEB candidates identified from Hα radial velocity variations. Upper limits to the new PCEB candidate orbital periods have been estimated in the same way as described in Rebassa-Mansergas et al. (2007). These values are given in Table 10.

12 SUMMARY

We have presented a catalogue of 1602 WDMS binaries from the spectroscopic SDSS DR6. We have used a decomposition/fitting technique to measure the effective temperatures, surface gravities, masses and distances to the white dwarfs, as well as the spectral types and distances to the companions in our catalogue. Distributions and density maps obtained from these stellar parameters have been used to study both the general properties and the selection effects of WDMS binaries in the SDSS. A comparison between the distances measured to the white dwarfs and the main-sequence companions shows $d_{sec} > d_{wd}$ for approximately one-fifth of the systems. We have also made use of *GALEX*, SDSS and UKIDSS magnitudes to study the distribution of WDMS binaries in colour–colour space and present simple colour cuts that allow us to clearly separate WDMS binaries from other stellar objects. Finally, we have measured radial velocities for 1068 WDMS binaries measured from the Na I $\lambda\lambda$8183.27, 8194.81 absorption doublet and/or the Hα emission line. Among the systems with multiple SDSS spectroscopy, we find five new WDMS binaries showing significant radial velocity variations identifying them as PCEB candidates. The new, updated and most complete catalogue of WDMS binaries from the SDSS presented here represents a superb data base for future follow-up studies that may significantly contribute to a better understanding of close compact binary star evolution.

ACKNOWLEDGMENTS

ARM acknowledges financial support from European Southern Observatory (ESO) and Gemini/Conicyt in the form of grant number 32080023. MRS thanks for support from FONDECYT (1061199). We thank the anonymous referee for his suggestions that helped improving the quality of the paper. We also thank Pierre Maxted for useful discussions.

REFERENCES

Abazajian K. N. et al., 2009, ApJ, 182, 543
Adelman-McCarthy J. K. et al., 2008, ApJS, 175, 297
Augusteijn T., Greimel R., van den Besselaar E. J. M., Groot P. J., Morales-Rueda L., 2008, A&A, 486, 843
Bianchi L. et al., 2007, ApJ, 173, 659
Bochanski J. J., West A. A., Hawley S. L., Covey K. R., 2007, AJ, 133, 531
Chiu K., Richards G. T., Hewett P. C., Maddox N., 2007, MNRAS, 375, 1180
Davis P. J., Kolb U., Willems B., Gänsicke B. T., 2008, MNRAS, 389, 1563
Davis P. J., Kolb U., Willems B., 2009, preprint (arXiv:0903.4152)
de Kool M., 1992, A&A, 261, 188
de Kool M., Ritter H., 1993, A&A, 267, 397
Dewi J. D. M., Tauris T. M., 2000, A&A, 360, 1043
Dye S. et al., 2006, MNRAS, 372, 1227
Eisenstein D. J. et al., 2006, ApJS, 167, 40
Fan X., 1999, ApJ, 117, 2528
Farihi J., Becklin E. E., Zuckerman B., 2005, ApJS, 161, 394
Gould A., Kollmeier J. A., 2004, ApJ, 152, 103
Hauschildt P. H., Baron E., 1999, J. Comput. Applied Math., 109, 41
Heller R., Homeier D., Dreizler S., Østensen R., 2009, A&A, 496, 191
Hewett P. C., Warren S. J., Leggett S. K., Hodgkin S. T., 2006, MNRAS, 367, 454
Holberg J. B., Sion E. M., Oswalt T., McCook G. P., Foran S., Subasavage J. P., 2008, ApJ, 135, 1225
Iben I. J., Livio M., 1993, PASP, 105, 1373
Koester D., Napiwotzki R., Voss B., Homeier D., Reimers D., 2005, A&A, 439, 317

Koester D., Kepler S. O., Kleinman S. J., Nitta A., 2009, J. Phys. Conf. Ser., 172, 012006
Lawrence A. et al., 2007, MNRAS, 379, 1599
Li N., Thakar A. R., 2008, Comput. Sci. Eng., 10, 18
Livio M., Soker N., 1988, ApJ, 329, 764
Makarova L., Karachentsev I., Takalo L. O., Heinaemaeki P., Valtonen M., 1998, A&AS, 128, 459
Martin D. C. et al., 2005, ApJ, 619, L1
Maxted P. F. L., Gänsicke B. T., Burleigh M. R., Southworth J., Marsh T. R., Napiwotzki R., Nelemans G., Wood P. L., 2009, MNRAS, 400, 2012
Morrissey P. et al., 2005, ApJ, 619, L7
Nagel T., Schuh S., Kusterer D.-J., Stahn T., Hügelmeyer S. D., Dreizler S., Gänsicke B. T., Schreiber M. R., 2006, A&A, 448, L25
Nebot Gómez-Morán A. et al., 2009, A&A, 495, 561
Nelemans G., Tout C. A., 2005, MNRAS, 356, 753
Politano M., Weiler K. P., 2006, ApJ, 641, L137
Politano M., Weiler K. P., 2007, ApJ, 665, 663
Pyrzas, S. et al., 2009, MNRAS, 394, 978
Raymond S. N. et al., 2003, AJ, 125, 2621
Rebassa-Mansergas A., Gänsicke B. T., Rodríguez-Gil P., Schreiber M. R., Koester D., 2007, MNRAS, 382, 1377
Rebassa-Mansergas A. et al., 2008, MNRAS, 390, 1635
Reid I. N., Cruz K. L., Allen P. R., 2007, ApJ, 133, 2825
Reid I. N., Cruz K. L., Kirkpatrick J. D., Allen P. R., Mungall F., Liebert J., Lowrance P., Sweet A., 2008, ApJ, 136, 1290
Richards G. T. et al., 2002, ApJ, 123, 2945
Schmidt G. D. et al., 2005, ApJ, 630, 1037
Schreiber M. R., Gänsicke B. T., 2003, A&A, 406, 305
Schreiber M., Nebot Gomez-Moran A., Schwope A., 2007, in Napiwotzki R., Burleigh R., eds, ASP Conf. Ser. Vol. 372, 15th European Workshop on White Dwarfs. Astron. Soc. Pac., San Francisco, p. 459
Schreiber M. R., Gänsicke B. T., Southworth J., Schwope A. D., Koester D., 2008, A&A, 484, 441
Schwope A. D., Nebot Gomez-Moran A., Schreiber M. R., Gänsicke B. T., 2009, A&A, 500, 867
Silvestri N. M. et al., 2006, AJ, 131, 1674
Silvestri N. M. et al., 2007, AJ, 134, 741
Smolčić V. et al., 2004, ApJ, 615, L141
Stoughton C. et al., 2002, AJ, 123, 485
Szkody P. et al., 2004, AJ, 128, 1882
Szkody P. et al., 2009, ApJ, 137, 4011
Taam R. E., Sandquist E. L., 2000, ARA&A, 38, 113
Vanden Berk D. E. et al., 2005, ApJ, 129, 2047
van den Besselaar E. J. M., Roelofs G. H. A., Nelemans G. A., Augusteijn T., Groot P. J., 2005, A&A, 434, L13
Webbink R. F., 1984, ApJ, 277, 355
Webbink R. F., 2008, in Milone E. F., Leahy D. A., Hobill D. W., eds, Astrophys. Space Sci. Libr. Vol. 352, Short-Period Binary Stars: Observations, Analyses, and Results. Springer, Berlin, p. 233
Willems B., Kolb U., 2004, A&A, 419, 1057
York D. G. et al., 2000, AJ, 120, 1579

SUPPORTING INFORMATION

Additional Supporting Information may be found in the online version of this article:

Table 2. Updated classification of the 204 objects from Silvestri et al. (2007) which are not considered as WDMS binaries by us.
Table 3. Updated classification of the 81 objects from Heller et al. (2009) which are not considered as WDMS binaries by us.
Table 5. The complete catalogue. Coordinates and *GALEX*–SDSS–UKIDSS magnitudes for the 1602 WDMS binaries and candidates are also included.
Table 7. White-dwarf masses, effective temperatures, surface gravities, spectral types and distances of the 1602 WDMS binaries in our catalogue, as determined from spectral modelling.
Table 9. Radial velocities measured from the Na I λλ8183.27, 8194.81 doublet and the Hα emission for 1068 systems in our catalogue.

Please note: Wiley-Blackwell are not responsible for the content or functionality of any supporting material supplied by the authors. Any queries (other than missing material) should be directed to the corresponding author for the article.

This paper has been typeset from a TEX/LATEX file prepared by the author.